ESC European Society of Cardiology
European Heart Journal (2025) **46**, 4988–5005
https://doi.org/10.1093/eurheartj/ehaf556

TRANSLATIONAL SCIENCE
Vascular biology and medicine

Excessive glycosylation drives thoracic aortic aneurysm formation through integrated stress response

Antonio Rochano-Ortiz [1], Irene San Sebastián-Jaraba [1,2], Carmen Zamora [1,3], Carolina Simó [4], Virginia García-Cañas [4], Sacramento Martínez-Albaladejo [1], María José Fernández-Gómez[1], Daniel Marcos-Ríos [1], Patricia Martínez-Núñez[1], Marta Martín-Lorenzo [5], Tiago R. Velho [6,7], María Jesús Ruíz-Rodríguez [8], Amanda Leal-Zafra[1,9], Enrique Gabandé-Rodríguez [10], Sara Martínez-Martínez [2,11], Andrea Guala [2,12,13], Óscar Lorenzo [1,14,15], Luis Miguel Blanco-Colio [1,2], José Luís Martín-Ventura [1,2,14], Gloria Álvarez-Llamas [5], Gonzalo Aldamiz-Echevarría [16], Gisela Teixidó-Tura [2,12,13], Alberto Forteza [2,3], Juan Francisco Nistal [2,17], Juan Miguel Redondo [2,10,11], Nerea Méndez-Barbero [1,2,9], María Mittelbrunn [10,*], and Jorge Oller [1,2,9,*]

[1]Laboratory of Vascular Pathology, Health Research Institute-Fundación Jiménez Díaz University Hospital, Universidad Autónoma de Madrid (IIS-FJD, UAM), 28040 Madrid, Spain; [2]Centro de Investigación Biomédica en Red de Enfermedades Cardiovasculares (CIBERCV), 28029 Madrid, Spain; [3]Department of Cardiac Surgery, University Hospital Puerta de Hierro, Majadahonda, Majadahonda, Spain; [4]Molecular Nutrition and Metabolism, Institute of Food Science Research (CIAL, CSIC-UAM), Madrid, Spain; [5]Department of Immunology, Health Research Institute-Fundación Jiménez Díaz University Hospital, Universidad Autónoma de Madrid (IIS-FJD, UAM), Madrid, Spain; [6]Department of Cardiothoracic Surgery, Hospital de Santa Maria, Centro Hospitalar Universitário, 1649-028 Lisboa, Portugal; [7]Cardiothoracic Surgery Research Unit, Centro Cardiovascular da Universidade de Lisboa (CCUL@RISE), Faculdade de Medicina da Universidade de Lisboa, Lisbon, Portugal; [8]Vascular Biology and Therapeutics Program, Yale School of Medicine, New Haven, CT, USA; [9]Facultad de Medicina y Biomedicina, Universidad Alfonso X el Sabio, 28691 Villanueva de la Cañada, Madrid, Spain; [10]Consejo Superior de Investigaciones Científicas (CSIC), Centro de Biología Molecular Severo Ochoa (CSIC-UAM), Universidad Autónoma de Madrid (UAM), 28049 Madrid, Spain; [11]Gene Regulation in Cardiovascular Remodeling and Inflammation Group, Centro Nacional de Investigaciones Cardiovasculares (CNIC), Madrid, Spain; [12]Department of Cardiology, Vall d'Hebron Hospital Universitari, Vall d'Hebron Barcelona Hospital Campus, Barcelona, Spain; [13]Cardiovascular Diseases, Vall d'Hebron Institut de Recerca (VHIR), Barcelona, Spain; [14]Faculty of Medicine, Universidad Autónoma de Madrid, Madrid, Spain; [15]CIBERDEM (Diabetes and Associated Metabolic Diseases Networking Biomedical Research Centre), Madrid, Spain; [16]Cardiac Surgery Service, Fundación Jiménez Díaz University Hospital-Universidad Autónoma de Madrid, Madrid, Spain; and [17]Cardiovascular Surgery, Hospital Universitario Marqués de Valdecilla, Instituto de Investigación Valdecilla (IDIVAL), Facultad de Medicina, Universidad de Cantabria, Santander, Spain

Received 9 October 2024; revised 1 April 2025; accepted 15 July 2025; online publish-ahead-of-print 28 July 2025

See the editorial comment for this article 'Sugar, stress, and the arterial wall: a metabolic link in aortic aneurysms', by F. Kirchhoff and L. Maegdefessel, https://doi.org/10.1093/eurheartj/ehaf586.

Abstract

Background and Aims Thoracic aortic aneurysms and dissections (TAADs) are depicted by aortic medial degeneration characterized by glycan-rich matrix accumulation. Marfan syndrome (MFS) is the most common inherited connective tissue disorder associated with TAAD. Although vascular smooth muscle cell metabolic dysfunction has emerged as a pathogenic driver of TAAD, surgical repair remains the mainstay of treatment. This study aimed to investigate the role of the hexosamine biosynthetic pathway (HBP) in sporadic and genetic TAAD pathophysiology.

Methods Hexosamine biosynthetic pathway activation was analysed in aortas from an MFS mouse model, a β-aminopropionitrile-induced non-genetic TAAD model, and patients with sporadic TAAD using transcriptomic and metabolomic approaches.

* Corresponding authors. Email: mmittelbrunn@cbm.csic.es (M.M.); Email: jorge.oller@iis-fjd.es (J.O.)

Aortic dilatation was monitored by ultrasound imaging. Pharmacological inhibition of HBP and integrated stress response (ISR) was performed to assess their therapeutic potential.

Results Hexosamine biosynthetic pathway was up-regulated in both an MFS mouse model and β-aminopropionitrile-induced TAAD, as well as in aortic samples from MFS and sporadic TAAD patients. Enhanced HBP activity contributed to aortic dilatation and medial degeneration via vascular smooth muscle cell dysfunction and ISR activation. Inhibition of HBP or ISR reversed these effects in the MFS model.

Conclusions The HBP–ISR axis drives medial degeneration in TAAD. These findings identify HBP and ISR as a potential target in TAAD of both genetic and non-genetic origin.

Structured Graphical Abstract

Key Question

What mechanisms drive the accumulation of the glycan-rich matrix in aortic medial degeneration, and contribute to the development of thoracic aortic aneurysms (TAA)?

Key Finding

- Hexosamine biosynthetic pathway (HBP) metabolites and glycosaminoglycans were elevated in aortic and blood samples from both Marfan mice and patients.
- Excessive HBP-driven glycosylation triggered the integrated stress response (ISR), leading to reduced protein translation and vascular smooth muscle cell dysfunction.

Take Home Message

The HBP–ISR axis may be a novel biomarker and therapeutic target for the prevention and treatment of TAA in Marfan syndrome and related diseases.

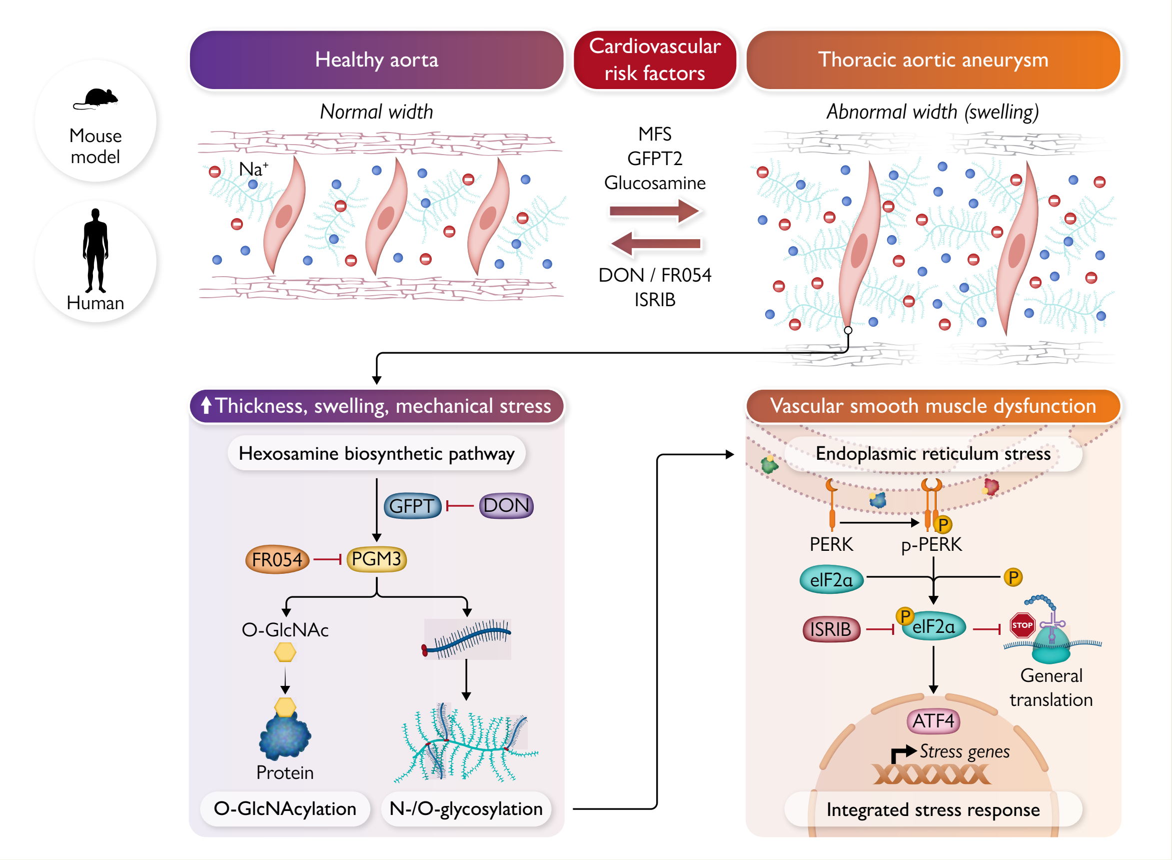

In thoracic aortic aneurysms and dissections, increased activity of the hexosamine biosynthetic pathway (HBP) promotes glycan-rich matrix accumulation via up-regulation of the rate-limiting enzyme glutamine-fructose-6-phosphate transaminase 2 (GFPT2). Exogenous glucosamine fuels the HBP, inducing aortic medial degeneration in wild-type mice. This glycan-rich matrix is characterized by a high negative charge, leading to increased accumulation of cations such as Na^+ raising osmotic pressure and contributing to medial thickening, elastin fragmentation, and mechanical stress. Additionally, excessive glycosylation driven by HBP activates the integrated stress response (ISR), reducing the canonical protein translation rate

and promoting activating transcription factor 4 (ATF4) translation. Pharmacological inhibition of HBP via DON/FR054 or ISR via ISR inhibitor (ISRIB) reverses aortic dilatation and medial degeneration in Marfan mice. Circulating HBP metabolites and glycosaminoglycans emerge as potential biomarkers in Marfan syndrome (MFS). The metabolic HBP–ISR axis emerges as a promising therapeutic target in thoracic aortic aneurysms and dissections.

Keywords Thoracic aortic aneurysm • Marfan Syndrome • Aortic medial degeneration • Hexosamine Biosynthetic pathway • Integrated stress response

Translational perspective

The accumulation of a glycan-rich matrix in the aortic media is a histological hallmark of thoracic aortic aneurysms and dissections (TAADs), particularly in Marfan syndrome. This glycosaminoglycan build-up has a deleterious effect on the micromechanical equilibrium essential for the proper function of elastic elements and optimal mechanotransduction. However, the precise molecular mechanisms underlying this glycan-rich matrix accumulation have remained elusive. The hexosamine biosynthetic pathway (HBP) is up-regulated in both non-genetic TAAD and a Marfan mouse models and patients. Hexosamine biosynthetic pathway contributes to the increase of the glycan-rich matrix in TAAD by supplying metabolites such as *N*-acetylglucosamine/*N*-acetylgalactosamine, thereby promoting aortic medial degeneration and dilatation. Elevated circulating HBP metabolites and glycosaminoglycans in Marfan patients highlight their potential as novel biomarkers. The excessive glycosylation driven by HBP activates the integrated stress response (ISR), reducing canonical protein synthesis and promoting vascular dysfunction. Hexosamine biosynthetic pathway metabolites could serve as circulating biomarkers, and HBP–ISR inhibitors may offer new clinical opportunities for treating TAAD in patients.

Introduction

Thoracic aortic aneurysms (TAAs) and dissections (TAADs) represent a primary cause of morbidity and mortality, highlighting the urgent need for pharmacological strategies to prevent aortic expansion and rupture.[1] Thoracic aortic aneurysm and dissection progression involves progressive aortic dilatation driven by vascular smooth muscle cell (VSMC) dysfunction and extensive extracellular matrix (ECM) remodelling.[1,2] While genetic factors play a pivotal role in approximately one in four cases, sporadic TAAD might result from hypertension, advanced age, male sex, or smoking.[3,4] Among inherited forms, Marfan syndrome (MFS; OMIM #154700), with an incidence of 1 in 5000 individuals, caused by dominant *FBN1* mutations, is the most prevalent.[5] Marfan syndrome patients commonly exhibit elongated bones, lens luxation, and unfortunately, a shortened life expectancy, with TAAD and rupture responsible for over 90% of MFS-related deaths.[6] Despite its clinical impact, pharmacologic options for TAAD remain limited, with surgery as the primary preventive intervention.[6,7]

Vascular smooth muscle cells constitute the predominant cell type within the aortic medial layer, regulate vascular tone, and maintain wall integrity. Vascular smooth muscle cells exhibit phenotypic plasticity, switching between contractile and secretory states. In the secretory phenotype, VSMCs increase ECM production and remodelling, altering wall mechanics and promoting aneurysm formation.[8–10]

Aortic medial degeneration, formerly termed cystic or medial necrosis degeneration, stands as a histological hallmark of TAAD.[11] Initially described by Babes and Mironescu in 1910, it has recently acquired significant attention.[12–15] Aortic medial degeneration is typified by the fragmentation of elastic fibres, fibrosis, excessive deposition of a glycan-mucoid matrix rich in proteoglycans (PGs) and glycosaminoglycans (GAGs). The elevated levels of PGs and GAGs are suggested to contribute to heightened stiffness and mechanical stress through their osmotic activity within the aortic wall. Broad research has established associations between aortic medial degeneration and hereditary vascular disorders, as well as vascular ageing.[16–18] Despite its significance, the molecular mechanisms underlying the accumulation of glycan-rich matrix in aortic medial degeneration and its impact on aortic homeostasis remain poorly understood.[19–21]

Previously, we have established that vascular metabolism contributes to aneurysm formation and rupture in both, genetic and sporadic aneurysm.[22–25] Here, we hypothesize that hyperactivation of the hexosamine biosynthetic pathway (HBP) drives aortic medial degeneration in TAAD. The HBP generates substrates for GAG and PG synthesis as well as post-translational protein modification via *O*-linked β-*N*-acetylglucosamine (*O*-GlcNac).[26,27] Increased glycosylation driven by HBP activates the integrated stress response (ISR), which, although initially protective, leads to maladaptive signalling and cellular dysfunction under chronic stress.[28–30]

Our study demonstrates that HBP activity drives aortic medial degeneration in TAAD. Conversely, treatment with HBP inhibitors restored aortic homeostasis in a murine model of MFS by reducing glycosylation levels, aortic medial degeneration, and ISR signalling. Additionally, administration of an ISR inhibitor in an MFS mouse model reversed TAAD, thereby improving aortic homeostasis. These findings highlight the potential of HBP and ISR as novel biomarkers, mediators, and therapeutic targets for the management of TAAD and other related conditions.

Methods

Detailed methods are provided in the Supplementary data online.

Results

The hexosamine biosynthetic pathway is increased in aortas of a murine model of Marfan syndrome

To elucidate the molecular mechanisms underlying aortic medial degeneration in MFS aortopathy, we re-analysed transcriptomic data from RNA-sequencing of aortas from *Fbn1*$^{C1041G/+}$ mice,[25] a well-established MFS model that replicates key features of the human disease, including syndromic features, aortic dilatation, and medial degeneration.[31] Aortas from 24-week-old *Fbn1*$^{+/+}$ and *Fbn1*$^{C1041G/+}$ mice were analysed, showing an intermediate stage of TAAD, when a clear aortic dilatation is observed, although at this age, they do not yet exhibit a terminal-stage aneurysm.[25,32] Transcriptomic profiling using ingenuity pathway analysis predicted increased activity of the HBP in the aortas of MFS mice, with a significant enrichment of genes related to UDP-*N*-acetyl-D-glucosamine

(UDP-GlcNAc) biosynthesis ($P = .047$). Although the HBP accounts for only 2%–5% of total glucose metabolism under basal conditions, it produces UDP-GlcNAc, a key substrate for *O*/*N*-glycosylation, a cornerstone for diverse cellular processes. Notably, UDP-GlcNAc is utilized for post-translational modification of intracellular proteins through *O*-GlcNAcylation (*O*-GlcNac) and also contributes to the synthesis and assembly of essential cellular components, including glycolipids, GAGs, PGs, and glycoproteins[26,27] (*Figure 1A* and *B*).

In MFS aortas, we observed the up-regulation of multiple HBP-related genes, including the inducible rate-limiting enzyme *Gfpt2* (glutamine-fructose-6-phosphate transaminase 2), as well as downstream enzymes such as *Uap1* (UDP-*N*-acetylglucosamine pyrophosphorylase 1) and *Gnpat1* (glucosamine-phosphate *N*-acetyltransferase 1; *Figure 1B*). Additionally, the enzymes *O*-GlcNAc transferase (*Ogt*) and *O*-GlcNAcase (*Oga*), which mediate the dynamic cycling of *O*-GlcNac on a wide array of proteins, were up-regulated (*Figure 1A* and *B*).[33] Our analysis also revealed an increase in Golgi enzymes involved in extracellular protein *N*-glycosylation, including alpha-1,3-mannosyl-glycoprotein 2-beta-*N*-acetylglucosaminyltransferase; *Mgat1*, *Mgat2*, *Mgat4a*, and *Mgat5b*, in MFS aortas (*Figure 1B*). Furthermore, the transcripts of genes, such as glucosamine UDP-*N*-acetyl-2-epimerase/*N*-acetylmannosamine kinase (*Gne*), UDP-GlcNAc:BetaGal Beta-1,3-*N*-acetylglucosaminyltransferase (*B3gnt3*), and hyaluronan synthase 1/3 (*Has1*/*Has3*), involved in the biosynthesis of *N*-acetylneuraminic acid, poly-*N*-acetyllactosamine chains, Sialyl–Lewis X (CD15s), and hyaluronic acid, respectively; and *Cd44* (hyaluronan receptor), were increased in MFS aortas (*Figure 1B*). These results were further corroborated by quantitative polymerase chain reaction analysis of aortic extracts from MFS mice (*Figure 1C*). Likewise, elevated *Gfpt2* mRNA levels were found in aortic VSMCs from MFS mice (Supplementary data online, *Figure S1A*). These findings suggest that the up-regulation of HBP and downstream enzymes may contribute to medial degeneration in MFS.

Additionally, we conducted an analysis of *Gfpt2* mRNA expression in MFS mice aortas across different ages. *Gfpt2* mRNA levels exhibit a significant increase at the very onset of MFS aortopathy, as early as 4 weeks old, in $Fbn1^{C1041G/+}$ mice, even when the aortic phenotype is barely detectable[25] (*Figure 1D*). Confocal immunostaining of MFS mice aortas further demonstrated an increase in Gfpt2, Uap1, and *O*-GlcNAc levels (*Figure 1E*). Immunoblot analysis of aortic samples from MFS mice revealed elevated protein levels of *O*-GlcNAc and Gfpt2 (*Figure 1F*; Supplementary data online, *Figure S1B*). Wheat germ agglutinin (WGA) staining, a marker for *N*-acetylglucosamine residues predominantly present in the ECM,[34] revealed enhanced extracellular glycosylation in the ascending aortas of MFS mice (*Figure 1G*).

In an effort to model MFS *in vitro*, we utilized lentiviral vectors to silence *Fbn1* expression in primary murine VSMCs[25] (Supplementary data online, *Figure S1C*). Consistent with the transcriptomic data obtained from MFS mice, VSMCs with silenced Fbn1 (*shFbn1*) exhibited elevated protein levels of Gfpt2 and Uap1 (*Figure 1H*; Supplementary data online, *Figure S1D*), alongside increased *Gfpt2* mRNA levels (Supplementary data online, *Figure S1C*). Furthermore, *shFbn1* VSMCs demonstrated increased levels of *O*-GlcNac as determined by immunoblot (*Figure 1H*; Supplementary data online, *Figure S1D*) and enhanced WGA and *O*-GlcNac staining analysed by flow cytometry analysis (Supplementary data online, *Figure S1E*).

These findings suggest that *FBN1* deficiency induces abnormal HBP activity, leading to increased levels of *O*-GlcNac and WGA staining in MFS aortopathy. These changes may contribute to the observed increase in GAGs and PGs shown in aortic medial degeneration.

Hexosamine biosynthetic pathway increase in murine and human sporadic thoracic aortic aneurysm samples

Both genetic and sporadic TAAD are characterized by aortic medial degeneration, accompanied by an accumulation of glycan-rich ECM. To assess whether the activation of the HBP is specific to MFS aortopathy or also occurs in non-genetic TAAD, we analysed a murine model of sporadic TAAD induced by treatment with the lysyl oxidase inhibitor, β-aminopropionitrile (BAPN).[35] Four-week-old male mice were treated with BAPN for 42 days (*Figure 2A*). This treatment led to a significant increase in ascending aortic diameter, exceeding 200% of the baseline diameter (*Figure 2B* and *C*), consistent with the development of TAAD. Histologically, BAPN administration induced aortic medial degeneration, characterized by elastin fibre disarray, as revealed by Elastin van Gieson staining. Additionally, Alcian blue staining demonstrated the accumulation of GAGs in the aortic wall (*Figure 2D*). To assess HBP activity, immunoblotting of aortic tissue showed elevated *O*-GlcNAc protein levels and expression of Gfpt2 (*Figure 2E*). Confocal microscopy further confirmed enhanced *O*-GlcNAcylation and WGA staining, indicating increased glycosylation within the aortic wall (*Figure 2F*), similarly to MFS mice aortas.

Next, we evaluated whether these findings extend to patients with sporadic TAA. Histological analysis demonstrated a significant increase in *O*-GlcNAc, WGA, and GFPT2 staining in affected human aortic samples (*Figure 2G* and *H*), supporting the notion that HBP activation and enhanced glycosylation are shared features of both genetic and sporadic TAAD.

Activation of the hexosamine biosynthetic pathway promotes aortic dilatation and medial degeneration in wild-type and Marfan syndrome mice

Given that excessive GAG-glycoprotein accumulation in aortic medial degeneration is a hallmark of TAAD,[11,14] we hypothesized that increased HBP activity contributes to the production of metabolites required for the PG and GAG medial accumulation during TAAD progression. To investigate this, we treated 20-week-old $Fbn1^{+/+}$ and $Fbn1^{C1041G/+}$ mice with glucosamine (GlcN) to fuel HBP (*Figure 3A*). Glucosamine is incorporated by the cells, phosphorylated to glucosamine-6-phosphate through hexokinases and converted to UDP-GlcNAc[26,36] (*Figure 1A*).

Glucosamine administration in drinking water for 28 days significantly increased ascending aortic diameter in wild-type mice (*Figure 3A–C*; Supplementary data online, *Figure S2A*). Notably, GlcN treatment exacerbated aortic dilatation in $Fbn1^{C1041G/+}$ mice compared with untreated controls (*Figure 3B* and *C*; Supplementary data online, *Figure S2A*). Histology revealed classical features of medial degeneration in GlcN-treated $Fbn1^{+/+}$ mice and worsened elastin architecture in $Fbn1^{C1041G/+}$, such as elastin fibre fragmentation and glycan-matrix accumulation (*Figure 3D* and *E*). Confocal analysis also revealed that GlcN increased HBP activity by *O*-GlcNac and WGA in aortic tissue from $Fbn1^{+/+}$ mice (*Figure 3F* and *G*).

To elucidate the potential role of GFPT2 up-regulation in the development of TAAD and medial degeneration, we transduced primary murine VSMCs with GFPT2 encoding lentiviral vectors (LV-GFPT2). GFPT2 transduction resulted in an increase in *O*-GlcNac levels

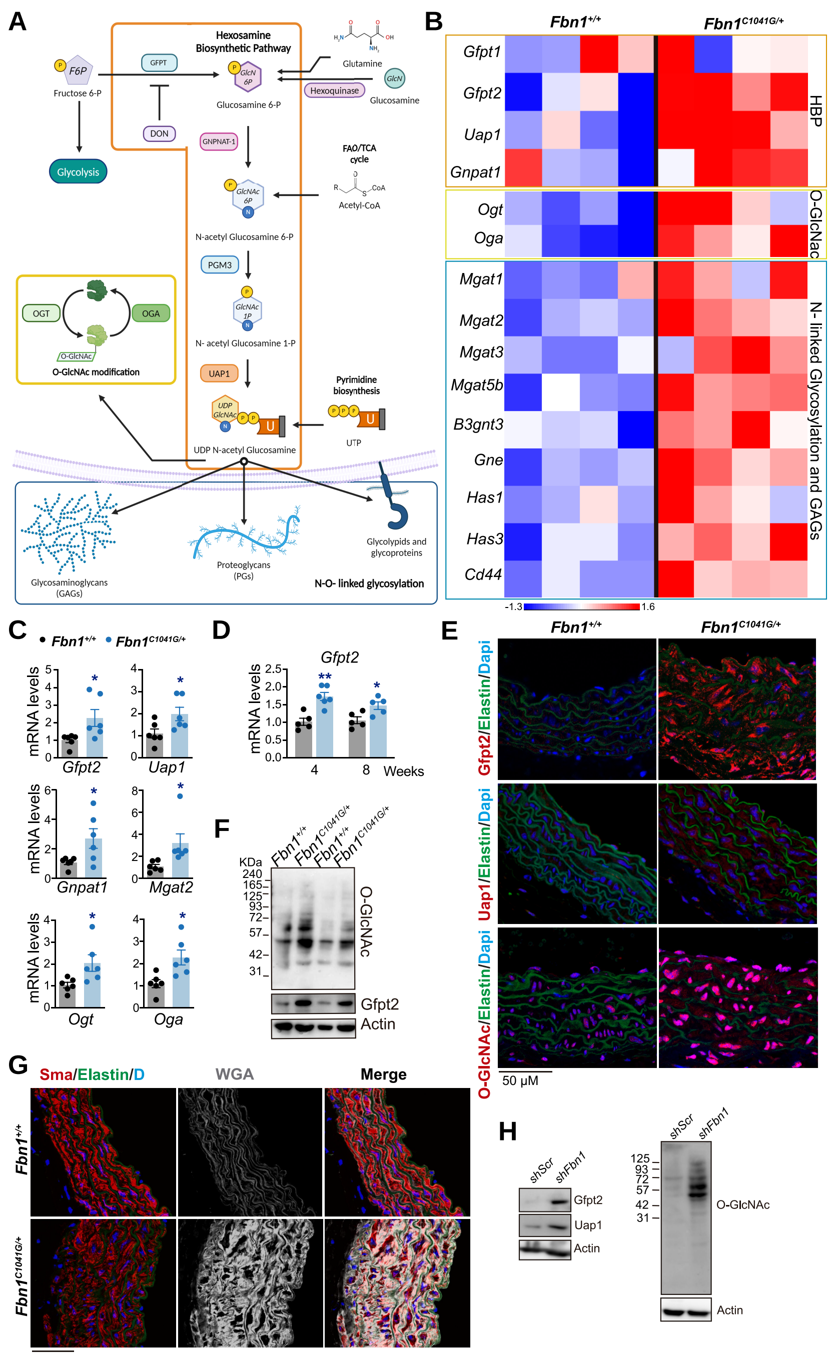

Figure 1 The hexosamine biosynthetic pathway genes are up-regulated in the aortas of a murine model Marfan syndrome. (*A*) Schematic of hexosamine biosynthetic pathway involvement in *O*-/*N*-linked glycosylation and glycosaminoglycan biosynthesis. (*B*) Heat map of hexosamine biosynthetic pathway, *O*-glycosylation, *N*-linked glycosylation, and GAG-related genes from RNA-sequencing analysis of aortic medial tissue from 24-week-old *Fbn1*$^{+/+}$ and *Fbn1*$^{C1041G/+}$ mice ($n = 4$). (*C*) Quantitative reverse transcription polymerase chain reaction analysis of *Gfpt2*, *Uap1*, *Gnpat1*, *Mgat2*, *Ogt*, *Oga* mRNA relative expression in aortic extracts from 20/24-week-old *Fbn1*$^{C1041G/+}$ and *Fbn1*$^{+/+}$ mice. (*D*) Quantitative reverse transcription polymerase chain reaction analysis of *Gfpt2* mRNA relative expression in aortic extracts from 4- or 8-week-old *Fbn1*$^{C1041G/+}$ and *Fbn1*$^{+/+}$ mice. (*E*) Representative confocal imaging of Gfpt2, Uap1, *O*-GlcNac (red); elastin (autofluorescence), and DAPI (4′,6-diamidino-2-phenylindole)-stained nuclei in the ascending aorta from 20-week-old *Fbn1*$^{C1041G/+}$ and *Fbn1*$^{+/+}$ mice ($n = 6$). (*F*) Representative immunoblot analysis of *O*-GlcNac proteins, Gfpt2 in aortic extracts from 20-week-old *Fbn1*$^{C1041G/+}$ and *Fbn1*$^{+/+}$ mice ($n = 6$). Actin was used as a loading control. (*G*) Representative confocal imaging of wheat germ agglutinin (grey), smooth muscle actin (Sma, red), elastin (green, autofluorescence), and DAPI-stained nuclei (blue) in the ascending aorta from 20-week-old *Fbn1*$^{C1041G/+}$ and *Fbn1*$^{+/+}$ mice ($n = 6$). (*H*) Representative immunoblot analysis of Gfpt2, Uap1, *O*-GlcNac proteins in extracts from primary murine vascular smooth muscle cells transduced with *shFbn1* or *shScr (ShControl)* for 5 days ($n = 3$). Actin was used as a loading control. Data are mean ± standard error of the mean. Student's *t*-test. *$P < .05$, **$P < .01$, ***$P < .001$ vs *Fbn1*$^{+/+}$ mice

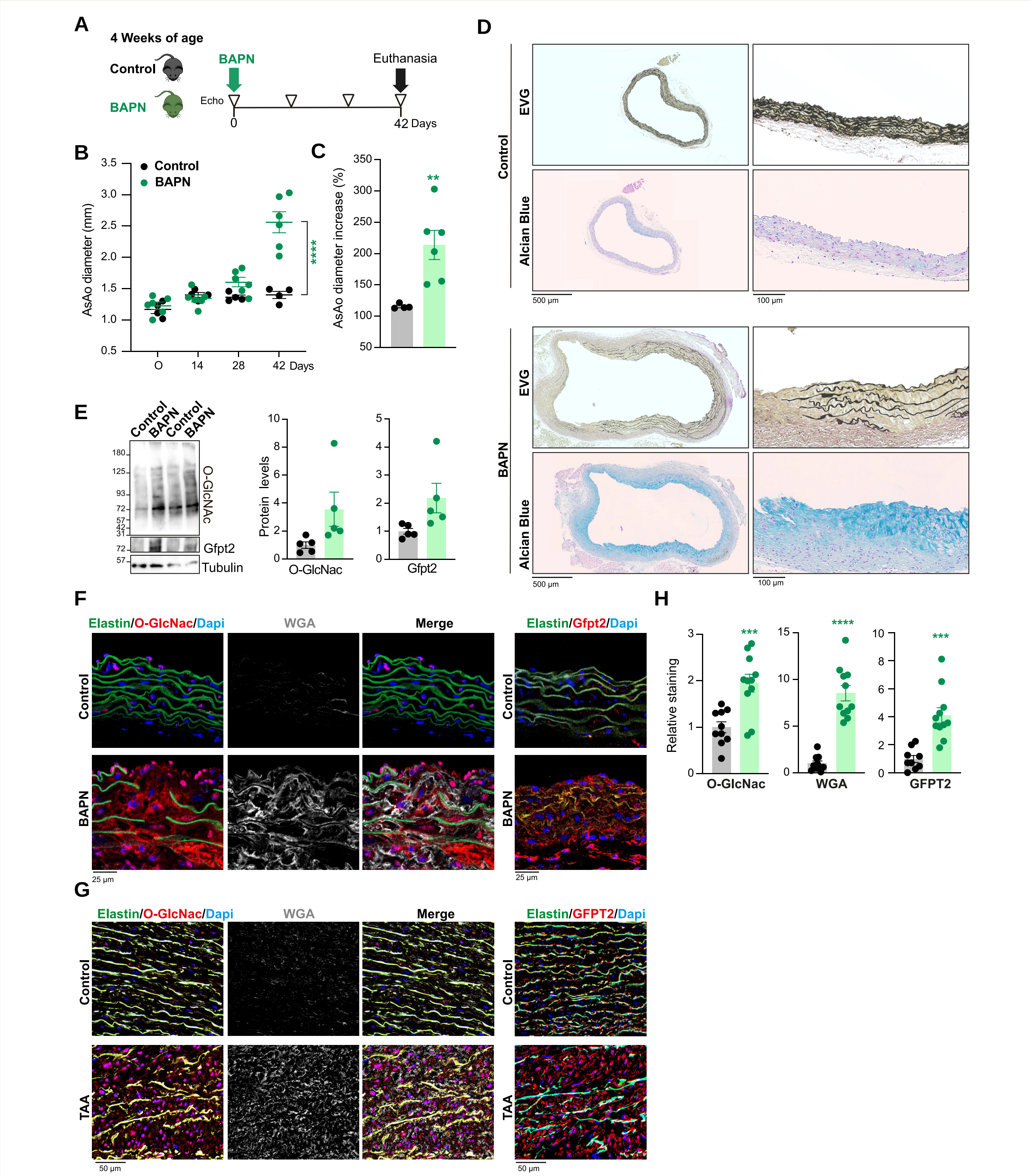

Figure 2 The hexosamine biosynthetic pathway is increased in the aortas of a murine model of sporadic thoracic aortic aneurysms and dissections and patients. (*A*) Experimental design, *A–F*, 4-week-old male C57/BL6 wild-type mice were treated with β-aminopropionitrile (0.5%) in drinking water for 42 days. (*B*) Evolution of maximal AsAo diameter (mm). (*C*) Percentage of increase of AsAo compared with baseline. (*D*) Representative histological staining of the ascending aorta with Elastin van Gieson and Alcian Blue. (*E*) Representative immunoblot analysis and quantification of *O*-GlcNac proteins, Gfpt2 in aortic extracts from 4-week-old control and β-aminopropionitrile-treated mice. Tubulin was used as a loading control. (*F*) Representative confocal imaging of Gfpt2, *O*-GlcNac; wheat germ agglutinin, elastin (autofluorescence), and DAPI-stained nuclei and quantification (*H*), in the ascending aorta from control and β-aminopropionitrile-treated mice. (*G*) Representative confocal immunostainings and quantification of *O*-GlcNac, GFPT2; and wheat germ agglutinin elastin (autofluorescence), and DAPI-stained nuclei in medial layer of aortic sections from control and sporadic non-genetic thoracic aortic aneurysms patients. Data are mean ± standard error of the mean. Student's *t*-test. $^{**}P < .01$, $^{***}P < .001$, $^{****}P < .001$ vs control

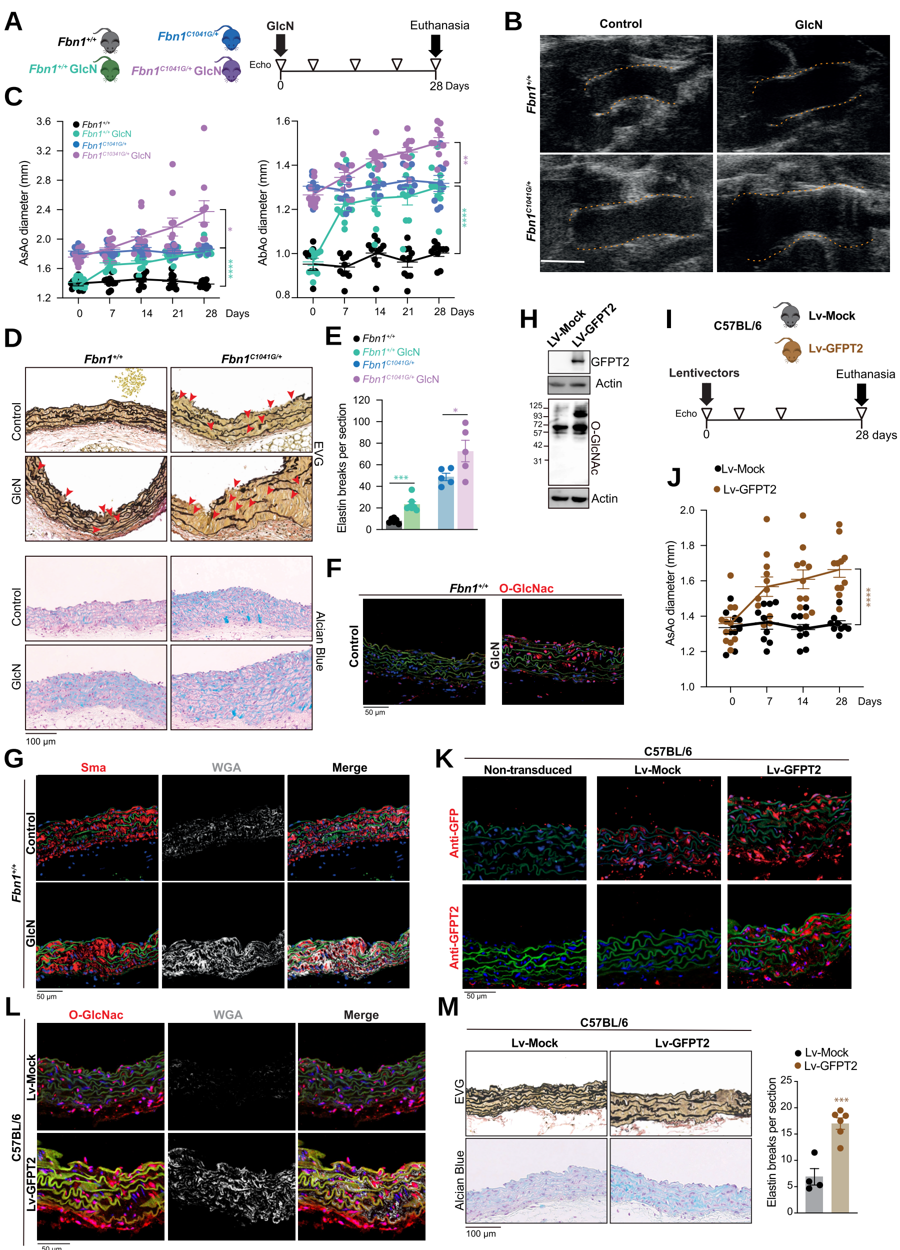

Figure 3 Boosting hexosamine biosynthetic pathway induces aortic dilatation and medial degeneration. (*A*) Experimental design, *A–E*, 20-week-old *Fbn1*$^{C1041G/+}$ and *Fbn1*$^{+/+}$ mice were with or without glucosamine in drinking water for 28 days. (*B*) Representative aortic ultrasound images after 28 days of control or glucosamine treatment. Discontinuous red lines mark the lumen boundary, scale bar 1 mm. (*C*) Evolution of maximal AsAo and AbAo diameter. (*D*) Representative histologic staining with Elastin van Gieson and Alcian blue in the AsAo and quantification of elastin breaks (*E*). (*F*) Representative confocal imaging of *O*-GlcNac proteins (red), elastin (green, autofluorescence), and DAPI-stained nuclei (blue) in the ascending aorta from *Fbn1*$^{+/+}$ mice treated with or without glucosamine for 28 days ($n = 6$). (*G*) Representative confocal imaging of wheat germ agglutinin, Smooth muscle actin (Sma), elastin (autofluorescence), and DAPI-stained nuclei in the ascending aorta from *Fbn1*$^{+/+}$ mice treated with/without glucosamine for 28 days ($n = 6$). (*H*) Representative immunoblot analysis of Gfpt2 and *O*-GlcNac proteins in LV-Mock (control) or Lv-GFPT2 transduced primary murine vascular smooth muscle cells for 5 days ($n = 3$). (*I*) Experimental design, *J–M*, 12-week-old C57BL/6 wild-type mice were injected with LV-Mock or Lv-GFPT2 lentivectors for 28 days. (*J*) Evolution of maximal AsAo diameter after inoculation of LV-Mock (control) or Lv-GFPT2 lentiviral vectors. (*K*) Representative confocal imaging GFP or GFPT2, elastin (autofluorescence), and DAPI-stained nuclei in ascending aortas from mice after 30 days of inoculation of LV-Mock (control) or Lv-GFPT2 lentivectors ($n = 6$). (*L*) Representative confocal imaging of wheat germ agglutinin, *O*-GlcNac proteins (red), elastin (autofluorescence), and DAPI-stained nuclei in ascending aortas from mice after 30 days of inoculation of LV-Mock (control) or Lv-GFPT2 lentivectors ($n = 6$). (*M*) Representative histologic staining with Elastin van Gieson and Alcian blue in the AsAo and quantification of elastin breaks in ascending aortas from mice after 30 days of inoculation of LV-Mock (control) or Lv-GFPT2 lentivectors. Data are mean ± standard error of the mean. Two-way repeated measurements analysis of variance (*C, J*), by one-way analysis of variance (*E*) or *t*-test (*M*). **P* < .05, ***P* < .01, ****P* < .001, *****P* < .0001 vs control

(*Figure 3H*). *In vivo* transduction in C57BL/6 wild-type mice (*Figure 3I*), resulted in increased GFPT2 expression and aortic diameter enlargement (*Figure 3J*; Supplementary data online, *Figure S2B*). Confocal analysis confirmed successful GFPT2 transduction and HBP activation, as evidenced by increased GFP, GFPT2, *O*-GlcNAc, and WGA staining (*Figure 3K and L*). GFPT2 transduction induced an increase in elastin breaks and glycan-matrix accumulation (*Figure 3M*).

These findings together suggest that excessive HBP activity resulting from GFPT2 up-regulation contributes to the accumulation of glycan matrix in aortic medial degeneration during TAAD development and is detrimental to aortic homeostasis.

The hexosamine biosynthetic pathway plays a critical role in the aortopathy of Marfan syndrome

To explore the therapeutic potential of inhibiting the HBP in TAAD, we first targeted the GFPT enzymes, which regulate the rate-limiting step of HBP. Given the absence of selective inhibitors, we employed 6-diazo-5-oxo-L-norleucine (DON), a well-established glutamine antagonist with high affinity for GFPT enzymes at nanomolar concentrations, over other glutamine-dependent enzymes (*Figure 1A*).[37,38] We treated *Fbn1*$^{C1041G/+}$ or *shFbn1* VSMCs with DON (5 nM) for 48 h. 6-Diazo-5-oxo-L-norleucine efficiently reduced levels of *O*-GlcNac and WGA, as evidenced by immunoblot and flow cytometry analysis (*Figure 4A*; Supplementary data online, *Figure S3A* and *B*). 6-Diazo-5-oxo-L-norleucine down-regulated expression of MFS-related genes, such as *Tgb1*, *Fgf2*, osteopontin (*Spp1*), and collagen 1 (*Col1a1*) in *shFbn1* VSMCs (Supplementary data online, *Figure S3C*).

We next tested whether DON infusion modulates HBP activity during aneurysm development in 20- to 22-week-old MFS mice over 28 days (*Figure 4B*). 6-Diazo-5-oxo-L-norleucine normalized aortic diameter in *Fbn1*$^{C1041G/+}$ mice (*Figure 4C and D*; Supplementary data online, *Figure S3D*), and restored histological features of aortic degeneration, including medial thickening, elastic fibre fragmentation, and deposition of glycan matrix (*Figure 4E and F*). *O*-GlcNAc and WGA levels were reduced in aortic tissue, as shown by immunoblot and confocal microscopy (*Figure 4G and H*). Notably, DON treatment normalizes GAGs and HBP metabolites in serum, including *N*-acetylglucosamine/*N*-acetylgalactosamine (GlcNac/GalcNac) and GlcN (*Figure 4I*). These results indicate that GFPT inhibition modulates pathogenic relevance to TAAD.

To achieve precise inhibition of the HBP, we employed FR054, a potent and selective inhibitor of phosphoacetylglucosamine mutase 3—an enzyme that converts GlcNAc-6-*P* to GlcNAc-1-P, (*Figure 1A*). By disrupting this critical biosynthetic step, FR054 lowers UDP-GlcNAc levels and reduces both *N*- and *O*-glycosylation, previously shown to be relevant in cancer progression.[39] *In vitro,* treatment with FR054 efficiently reduced levels of *O*-GlcNAc and WGA in *Fbn1*$^{C1041G/+}$ VSMCs, as evidenced by flow cytometry analysis (*Figure 5A*), and decreased expression of MFS-associated genes, including *Spp1*, *Fgf2*, in aortic VSMCs from *Fbn1*$^{C1041G/+}$ mice (*Figure 5B*). To assess the *in vivo* efficacy of FR054, it was infused via osmotic minipumps in 18- to 20-week-old MFS mice for 28 days (*Figure 5C*). FR054 normalized aortic dilatation in *Fbn1*$^{C1041G/+}$ mice (*Figure 5D*; Supplementary data online, *Figure S4*) and restored the histological features of aortic degeneration in MFS, such as elastic fibre fragmentation and glycan-matrix accumulation (*Figure 5E*). Moreover, FR054 treatment reduced *O*-GlcNAc and WGA staining in aortic tissue (*Figure 5F*), serum GAG levels (*Figure 5G*), and aortic expression of *Col1a1* and *Klf4* mRNA in aortas from *Fbn1*$^{C1041G/+}$ mice (*Figure 5H*).

These data indicate that HBP inhibition, decreases serum GAGs and HBP metabolites, aortic glycosylation levels, thereby reducing aortic medial degeneration, improving aortic architecture, and restoring homeostasis in MFS aortopathy.

The integrated stress response is activated by the hexosamine biosynthetic pathway in thoracic aortic aneurysm

RNA-sequencing analysis of aortas from 24-week-old MFS mice revealed the activation of endoplasmic reticulum stress pathway ($P = .032$, Z-score $= 1.342$), including increased expression of *Atf4*, *Atf3*, *Atf6*, *Chop*, *Xbp1*, chaperones *Hspb1*, *Hspa5*, *Hspb7*, *Dnajc3*, and *prolyl 4-hydroxylase* (*P4hb*) (*Figure 6A*). Endoplasmic reticulum stress occurs when misfolded proteins accumulate, activating the ISR via protein kinase R (PKR)-like endoplasmic reticulum kinase (PERK) phosphorylation. Under stress, BiP dissociates from PERK, enabling its phosphorylation and subsequent eIF2α phosphorylation, which suppresses global translation while promoting selective ATF4 translation.[28] Hexosamine biosynthetic pathway activation via GFPT up-regulation has been shown to induce ISR.[29] Likewise, DON reduces endoplasmic reticulum stress induced by GFPT overexpression or GlcN treatment.[40]

To investigate the relationship between ISR and HBP in VSMCs, *shFbn1*-VSMCs were treated with DON for 48 h, which led to reduced p-eIF2α and decreased Atf4 and Atf6 expression (Supplementary data online, *Figure S5A* and *B*). *In vivo*, 28-day DON treatment in *Fbn1*$^{C1041G/+}$ mice reduced aortic p-PERK, p-eIF2α, and ATF4 immunostaining (*Figure 6B*), consistent with ISR inhibition. Immunoblots confirmed decreased levels of *O*-GlcNac, p-Perk, p-eIF2α, and Atf4 (*Figure 6C*), along with reduced mRNA expression of *Atf4* and *Atf6*; and Atf4-response gene *Tgfb2* (*Figure 6D*). These data indicate that ISR is activated in MFS mice and attenuated by DON treatment.

To characterize the molecular impact of DON treatment, we conducted RNA-sequencing analysis on aortas from *Fbn1*$^{+/+}$ and *Fbn1*$^{C1041G/+}$ mice treated with or without DON for 28 days ($n = 4$). 6-Diazo-5-oxo-L-norleucine treatment led to decreased expression of genes associated with the ISR, including *Atf4* and its downstream targets such as *Chop*, *Xbp1*, *Hsp90b1*, *Ankrd3*, *Arhfap23*, *Hyou1*, *Iars1*, *Igfp7*, Cyclooxygenase-2 (*Ptgs2*), and *Tgfb2* (*Figure 6E*). Remarkably, IPA predicted a reduction in the Transforming Growth Factor beta (TGF-β) pathway activity, with a significant decrease in TGF-β upstream regulator activation ($P = 2.57 \times 10^{-11}$; activation Z-score $= -9.913$). The DON treatment down-regulated key MFS-related genes, including *Tgfb3*, *Cnn2*, *Serpine1*, *Thbs1*, *Pdgf*; and the PGs *Acan*, *Vcan*, and *Sdc4* (*Figure 6E*).

Similarly, FR054 infusion for 28 days in *Fbn1*$^{C1041G/+}$ mice reduced ISR markers, including p-Perk, p-Eif2α, and Atf4 in aortic immunostainings (Supplementary data online, *Figure S6A*), as well as *Atf4*, *Atf6*, and *Tgfb2* mRNA levels (Supplementary data online, *Figure S6B*). These findings suggest that HBP inhibition in MFS with either FR054 or DON, suppresses ISR signalling in MFS aortas.

To confirm that excessive HBP activity induces ISR in VSMCs, we analysed p-eIF2α and Atf4 and Atf6 levels in VSMCs transduced with a LV-GFPT2 (Supplementary data online, *Figure S5C* and *D*). *In vivo*, GlcN treatment or GFPT2-overexpression in wild-type mice for 28 days induced ISR activation, evidenced by an increase in p-Perk, p-eIF2α, and Atf4 aortic immunostainings (*Figure 6F and G*).

These findings indicate that excessive protein glycosylation induced by HBP triggers ISR signalling in aortas from wild-type and MFS mice.

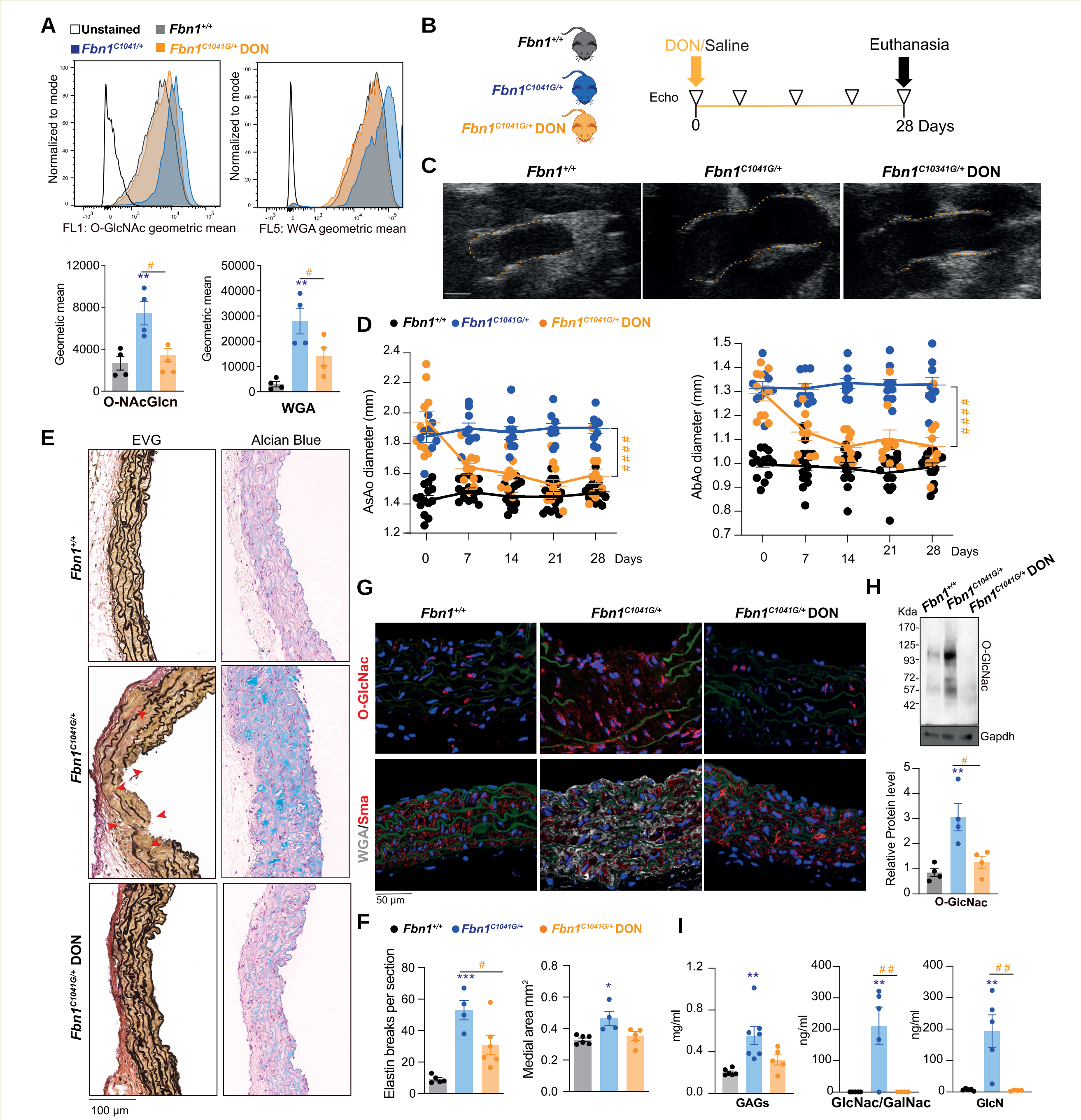

Figure 4 Hexosamine biosynthetic pathway inhibition by 6-diazo-5-oxo-L-norleucine restores aortic dilatation and medial degeneration in Marfan syndrome mice. (*A*) Representative flow cytometry histograms and statistical analysis of *O*-GlcNAc and wheat germ agglutinin staining of primary vascular smooth muscle cells from *Fbn1*$^{C1041G/+}$ and *Fbn1*$^{+/+}$ mice treated with or without 6-diazo-5-oxo-L-norleucine for 24 h. (*B*) Experimental design, *B–J*, 20/22-week-old *Fbn1*$^{C1041G/+}$ and *Fbn1*$^{+/+}$ mice were infused with minipumps with saline (control) or 6-diazo-5-oxo-L-norleucine for 28 days. (*C*) Representative aortic ultrasound images after 28 days of control or 6-diazo-5-oxo-L-norleucine treatment. Discontinuous red lines mark the lumen boundary, scale bar 1 mm. (*D*) Evolution of maximal AsAo and AbAo diameter. (*E*) Representative histological staining with Elastin van Gieson and Alcian blue in the AsAo, quantification of elastin breaks and aortic medial thickness (*F*) ($n = 6$). (*G*) Representative confocal imaging of *O*-GlcNac proteins or SMA, wheat germ agglutinin, elastin (autofluorescence), DAPI-stained nuclei in the ascending aorta from *Fbn1*$^{+/+}$ and *Fbn1*$^{C1041G/+}$ mice treated with/without 6-diazo-5-oxo-L-norleucine for 28 days ($n = 6$). (*H*) Representative immunoblot analysis and quantification of *O*-GlcNac proteins in aortic extracts from *Fbn1*$^{C1041G/+}$ and *Fbn1*$^{+/+}$ mice with saline or 6-diazo-5-oxo-L-norleucine for 28 days ($n = 4$). (*I*) Glycosaminoglycans serum levels, *N*-acetylglucosamine/*N*-acetylglucosamine and glucosamine in sera from 20-week-old *Fbn1*$^{C1041G/+}$ and *Fbn1*$^{+/+}$ mice with saline or 6-diazo-5-oxo-L-norleucine for 28 days. Data are mean ± standard error of the mean. One-way analysis of variance (*A, F, H, I*) or two-way repeated measurements analysis of variance (*D*). *$P < .05$, **$P < .01$, ***$P < .001$, for *Fbn1*$^{C1041G/+}$ vs *Fbn1*$^{+/+}$; #$P < .05$, ##$P < .01$, ####$P < .0001$ for *Fbn1*$^{C1041G/+}$ DON vs *Fbn1*$^{C1041G/+}$

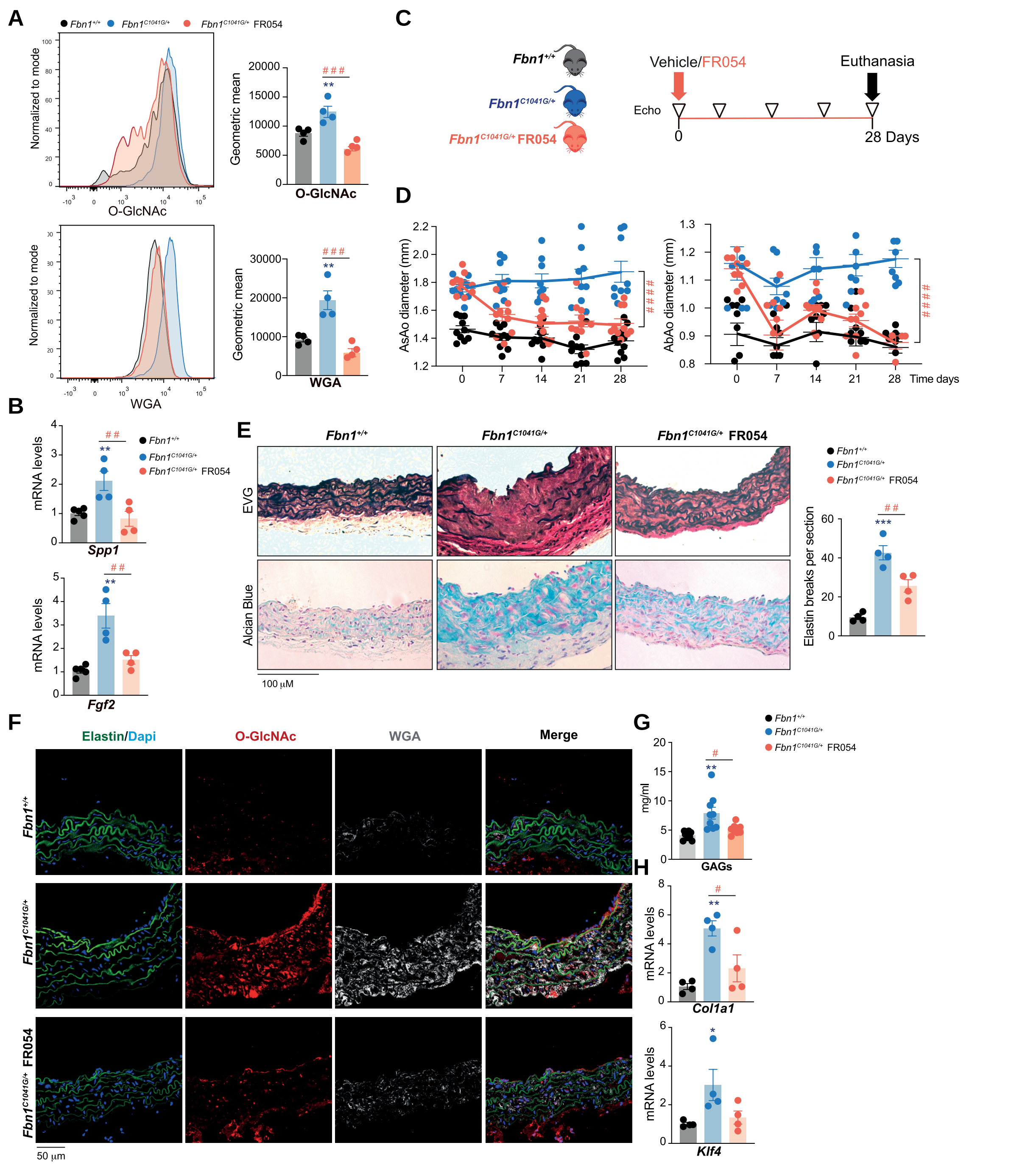

Figure 5 Phosphoacetylglucosamine mutase 3 (PGM3) inhibition by FR054 decreases aortic dilatation and glycans in Marfan syndrome aortas. (*A*) Representative flow cytometry histograms and statistical analysis of *O*-GlcNAc and wheat germ agglutinin staining of primary vascular smooth muscle cells from *Fbn1*$^{C1041G/+}$ and *Fbn1*$^{+/+}$ mice treated with or without FR054 100 μM for 48 h. (*B*) Quantitative reverse transcription polymerase chain reaction analysis of *Spp1* and *Fgf2* mRNA relative expression in extracts from vascular smooth muscle cells of *Fbn1*$^{C1041G/+}$ and *Fbn1*$^{+/+}$ mice treated with or without FR054 100 μM for 48 h. (*C*) Experimental design, *D–H*, 18/20-week-old *Fbn1*$^{C1041G/+}$ and *Fbn1*$^{+/+}$ mice were infused with minipumps with saline (control) or FR054 for 28 days. (*D*) Evolution of maximal AsAo and AbAo diameter. (*E*) Representative histologic staining with Elastin van Gieson and Alcian blue in the AsAo and quantification of elastin breaks. (*F*) Representative confocal imaging of *O*-GlcNac proteins or SMA, wheat germ agglutinin, elastin (autofluorescence), DAPI-stained nuclei in the ascending aorta from *Fbn1*$^{+/+}$ and *Fbn1*$^{C1041G/+}$ mice treated with/without 6-diazo-5-oxo-L-norleucine for 28 days ($n = 6$). (*G*) Glycosaminoglycans serum from *Fbn1*$^{C1041G/+}$ and *Fbn1*$^{+/+}$ mice with saline or FR054 for 28 days. (*H*) Quantitative reverse transcription polymerase chain reaction analysis of *Col1a1* and *KLF4 mRNA* relative expression in aortic extracts from *Fbn1*$^{C1041G/+}$ and *Fbn1*$^{+/+}$ mice treated with or without FR054 28 days. Data are mean ± standard error of the mean. One-way analysis of variance (*A*, *B*, *E*, *G*, *H*) or two-way repeated measurements analysis of variance (*D*). $*P < .05$, $**P < .01$, $***P < .001$, for *Fbn1*$^{C1041G/+}$ vs *Fbn1*$^{+/+}$; #$P < .05$, ##$P < .01$, ####$P < .0001$ for *Fbn1*$^{C1041G/+}$ DON vs *Fbn1*$^{C1041G/+}$

The integrated stress response is involved in vascular smooth muscle cell dysfunction in Marfan syndrome

The ISR regulates canonical protein translation rate and orchestrates a protective response, aiming to maintain cellular homeostasis and organismal fitness.[28] To assess ISR activation in MFS, we transduced VSMCs from *Fbn1*$^{C1041G/+}$ and *Fbn1*$^{+/+}$ mice, as well as wild-type *shControl* and *shFbn1*, with a lentiviral ATF4-translation reporter carrying ATF4-5′-UTR fused to Scarlet fluorescent protein (LV-ATF4Scarlet).[41] Both *shFbn1*-VSMCs and VSMCs from *Fbn1*$^{C1041G/+}$ mice exhibited an increase in Scarlet fluorescence compared with controls, indicating enhanced ATF4 translation (*Figure 7A*; Supplementary data online, *Figure S7A*). Treatment with DON (24 h) reduced Scarlet fluorescence in VSMCs-*Fbn1*$^{C1041G/+}$, involving HBP in ATF4 translation (*Figure 7A*).

Next, we evaluated the role of ISR in MFS using the ISR inhibitor (ISRIB), which reverses the effects of p-eIF2α and has been investigated in various neurodegenerative mouse models.[28,42] Integrated stress response inhibitor treatment for 24 h in *shFbn1*-VSMCs reduced levels of *Atf4* and *Atf6* mRNA (Supplementary data online, *Figure S7B*). Likewise, ISRIB treatment for 24 h decreased Scarlet fluorescence in VSMCs-*Fbn1*$^{C1041G/+}$ transduced with LV-ATF4Scarlet, confirming ISR involvement in ATF4 translation (*Figure 7A*). Since ISR inhibits canonical protein translation, via phosphorylation of eIF2α, we next assessed translation rate in MFS, using puromycin, an antibiotic that incorporates into nascent proteins and enables visualization of active ribosomes.[43,44] Following a 5 min puromycin pulse, *Fbn1*$^{C1041G/+}$, displayed reduced puromycylated proteins compared with *Fbn1*$^{+/+}$ cells, indicating lower translation rates (*Figure 7B*). Conversely, treatment with DON or ISRIB for 24 h in *Fbn1*$^{C1041G/+}$ VSMCs increased puromycin-labelled proteins (*Figure 7B*; Supplementary data online, *Figure S8A*). Furthermore, FR054 also led to a decrease of *Atf4* and *Tgfb2* mRNA levels in *Fbn1*$^{C1041G/+}$ VSMCs (Supplementary data online, *Figure S8B*).

Subsequently, we evaluated the possible role of ISR in MFS-aortic pathology *in vivo* by infusing 20/22-week-old *Fbn1*$^{C1041G/+}$ mice with ISRIB for 28 days (*Figure 7C*). Integrated stress response inhibitor normalized aortic diameter (*Figure 7D and E*; Supplementary data online, *Figure S8*), and improved aortic histology, with reduced elastic fibre fragmentation and diminished Alcian blue staining in MFS mice (*Figure 7F and G*). ATF4 protein levels were decreased, as shown by immunostaining and immunoblot (*Figure 7H and I*) along with decreased mRNA expression of IRS-induced genes *Atf4*, *Atf6*, and *Tgfb2* (*Figure 7J*).

These data suggest that maladaptive ISR mediates aortic pathology in MFS aortopathy.

Hexosamine biosynthetic pathway and integrated stress response axis in aortas from patients with Marfan syndrome

Next, we investigated whether the involvement of HBP and ISR extends to MFS patients. Histological analysis of *O*-GlcNac and WGA staining confirmed a significant increase in HBP activity in human aortic MFS samples (*Figure 8A and B*). In two independent cohorts, MFS patients exhibited elevated serum and plasma levels of GAGs compared with controls (*Figure 8C*). Metabolomic analysis confirmed increased circulating HBP metabolites, specifically GlcNAc/GalNAc and GlcN in plasma from MFS patients (*Figure 8D*). Furthermore, immunostaining of GFPT2 was significantly higher in the medial layer of MFS patients compared with controls (*Figure 8E and F*). Notably, p-PERK, p-EIF2α, and ATF4 immunostainings revealed robust activation of ISR in MFS patients (*Figure 8E and F*).

Taken together, these findings support the notion that the HBP–ISR axis may serve as important molecular markers and mediators of aortic pathology in human TAAD. Consequently, the evaluation of HBP–ISR inhibitors for the treatment of TAAD is warranted (*Figure 8G*).

Discussion

Despite the high incidence and mortality associated with TAAD, no pharmacological treatments currently prevent disease progression or dissection. Current pharmacological approaches focus on blood pressure control using β-adrenergic blockers or the angiotensin II receptor-1 antagonist losartan, which can slow aortic dilatation but does not prevent dissection.[45,46] Consequently, TAAD management relies on surgical prophylactic repair, which carries substantial peri-operative mortality and morbidity.[47] There is a clear need to identify molecular drivers of TAAD to develop targeted therapies.[1,7]

We demonstrate that glycoprotein, PG, and GAG accumulation in TAAD is driven by enhanced HBP activity (*Structured Graphical Abstract*). Hexosamine biosynthetic pathway is a minor branch of glucose metabolism responsible for protein glycosylation.[26] Although glucose flux through the HBP is minimal in homeostasis, it significantly increases in pathologies such as diabetes, cancer and cardiac hypertrophy.[26] Acting as a nutrient-sensing pathway, HBP integrates multiple metabolic pathways such as sugars (glucose), amino acids (glutamine), nucleotides (UTP), and fatty acids (acetyl-CoA),[26] influencing signalling pathways, including mTOR and AMPK, which contribute to pathophysiological alterations in aortic aneurysms.[48–50]

GFPT catalyses the conversion of glutamine and fructose-6-phosphate into glucosamine-6-phosphate and glutamate. There are two mammalian paralogs of GFPT: GFPT1 and GFPT2, which share a high degree of sequence similarity, ranging from 75% to 80%. GFPT2 is expressed and induced in various cell types, including mouse embryonic stem cells and cardiomyocytes, macrophages. Notably, GFPT2 has been identified as a biomarker for poor prognosis in some malignancies.[26,27,51] Unlike GFPT1, GFPT2 synthesizes glucosamine-6-phosphate more slowly but is not vulnerable to UDP-GlcNAc feedback inhibition. GFPT2 is inducible by Nuclear factor kappa-light-chain-enhancer of activated B cells (NF-κB)[52] and TGF-β[53] pathways, while GFPT1 is ubiquitously expressed.[27] Additionally, GFPT2 is involved in a TGF-β-pathway positive feedback loop that amplifies Protein kinase B or AKT[36] and TGF-β[54] signalling pathways in cardiac fibrosis and hypertrophy. Importantly, we found that both murine and human MFS show a marked increase in GFPT2 expression.

Our primary objective was to inhibit Gfpt2, given its elevated expression levels in MFS aortas. In the absence of specific inhibitors for GFPT, we utilized DON, a potent glutamine antagonist known to inhibit glycosylation processes.[27,38] Our results indicate that glutamine metabolism is involved in MFS pathology. Subsequently, to achieve a more precise inhibition of the HBP, we employed FR054, which specifically targets a central enzyme in the HBP.[39] Notably, the effects of FR054 treatment were comparable with those observed with DON. As an alternative approach, we increased exogenously HBP activity in wild-type animals by overexpressing GFPT2 via lentiviral vectors or administering oral GlcN. Both approaches mimicked the aortic medial degeneration of the MFS-aortic phenotype.

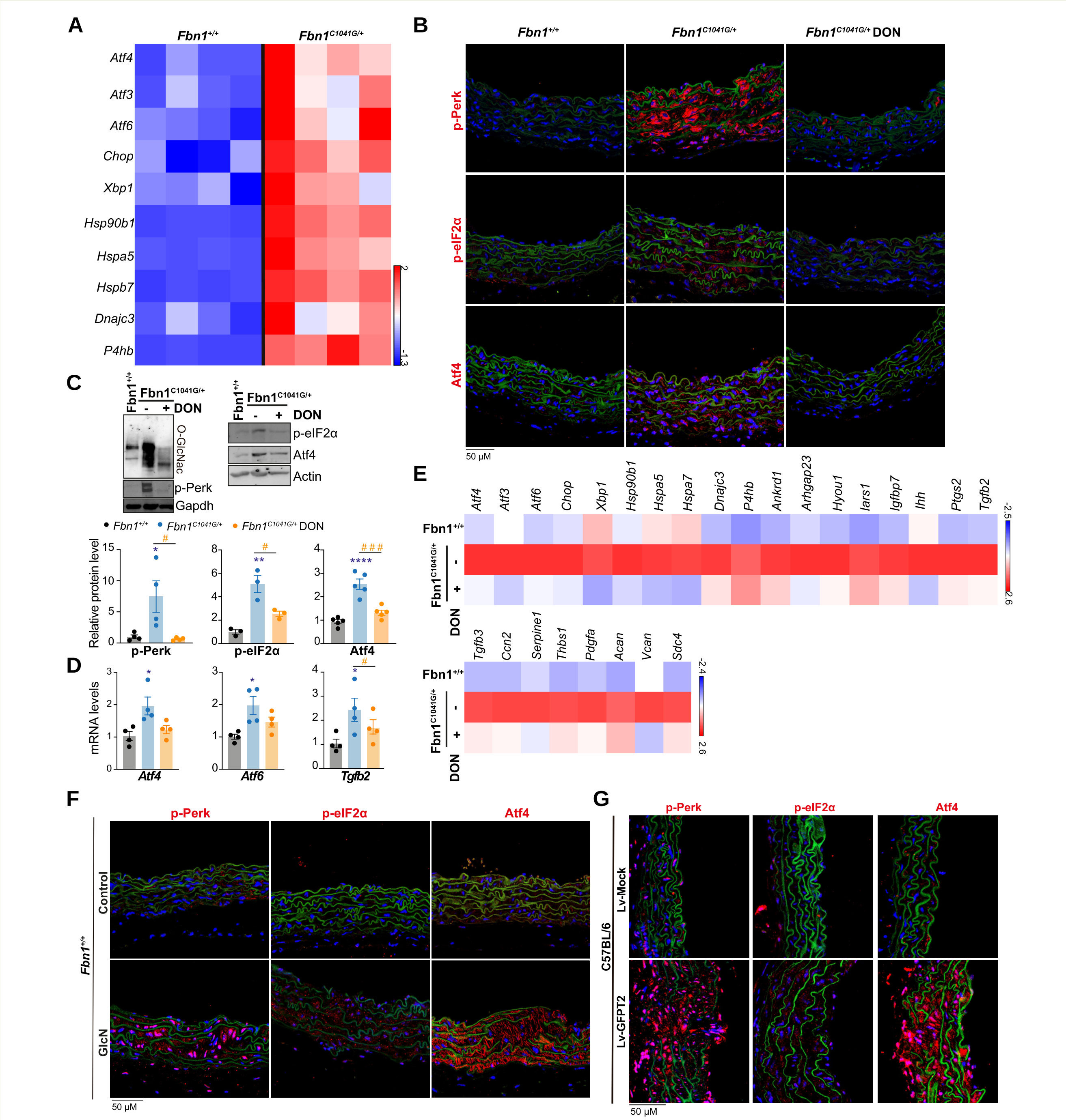

Figure 6 Integrated stress response is activated by hexosamine biosynthetic pathway in aortic tissue. (*A*) Heat map of integrated stress response–related genes from RNA-Sequencing analysis of aortic medial tissue from 24-week-old *Fbn1*$^{+/+}$ mice ($n = 4$) and from *Fbn1*$^{C1041G/+}$ mice ($n = 4$). (*B*) Representative confocal imaging p-Perk, p-eIF2α, or atf4 (red); elastin (autofluorescence), and DAPI-stained nuclei in ascending aortas from 20-week-old *Fbn1*$^{C1041G/+}$ and *Fbn1*$^{+/+}$ mice infused with saline or 6-diazo-5-oxo-L-norleucine for 28 days ($n = 5$). (*C*) Representative immunoblot analysis and quantification of *O*-GlcNac proteins, p-Perk p-eIF2a, or Atf4 in aortic extracts from 20-week-old *Fbn1*$^{C1041G/+}$ and *Fbn1*$^{+/+}$ mice infused with saline or 6-diazo-5-oxo-L-norleucine for 28 days. (*D*) Quantitative reverse transcription polymerase chain reaction analysis of *Atf4*, *Atf6*, and *Tgfb2* mRNA relative expression in aortic extracts from 20/24-week-old *Fbn1*$^{C1041G/+}$ and *Fbn1*$^{+/+}$ mice treated for 28 days with 6-diazo-5-oxo-L-norleucine . (*E*) Heat map of integrated stress response–related and extracellular matrix–related genes from RNA-sequencing analysis of aortic medial tissue from 20-week-old *Fbn1*$^{+/+}$ mice ($n = 4$) and from *Fbn1*$^{C1041G/+}$ mice infused with saline or 6-diazo-5-oxo-L-norleucine for 28 days ($n = 4$). (*F*) Representative confocal imaging p-Perk, p-eIF2α, or Atf4; elastin (autofluorescence), and DAPI-stained nuclei in ascending aortas from 20/22-week-old *Fbn1*$^{+/+}$ mice treated with or without glucosamine for 28 days ($n = 6$). (*G*) Representative confocal imaging p-Perk, p-eIF2α, or Atf4 elastin (green, autofluorescence), and DAPI-stained nuclei in ascending aortas from 20-week-old *Fbn1*$^{+/+}$ mice transduced with LV-Mock or LV-GPFT2 for 30 days ($n = 5$). Data are mean ± standard error of the mean. One-way analysis of variance *$P < .05$, **$P < .01$ or ***$P < .001$ for *Fbn1*$^{C1041G/+}$ vs *Fbn1*$^{+/+}$; #$P < .05$ or ###, ##$P < .01$, $P < .001$ for *Fbn1*$^{C1041G/+}$ FR054 vs *Fbn1*$^{C1039G/+}$

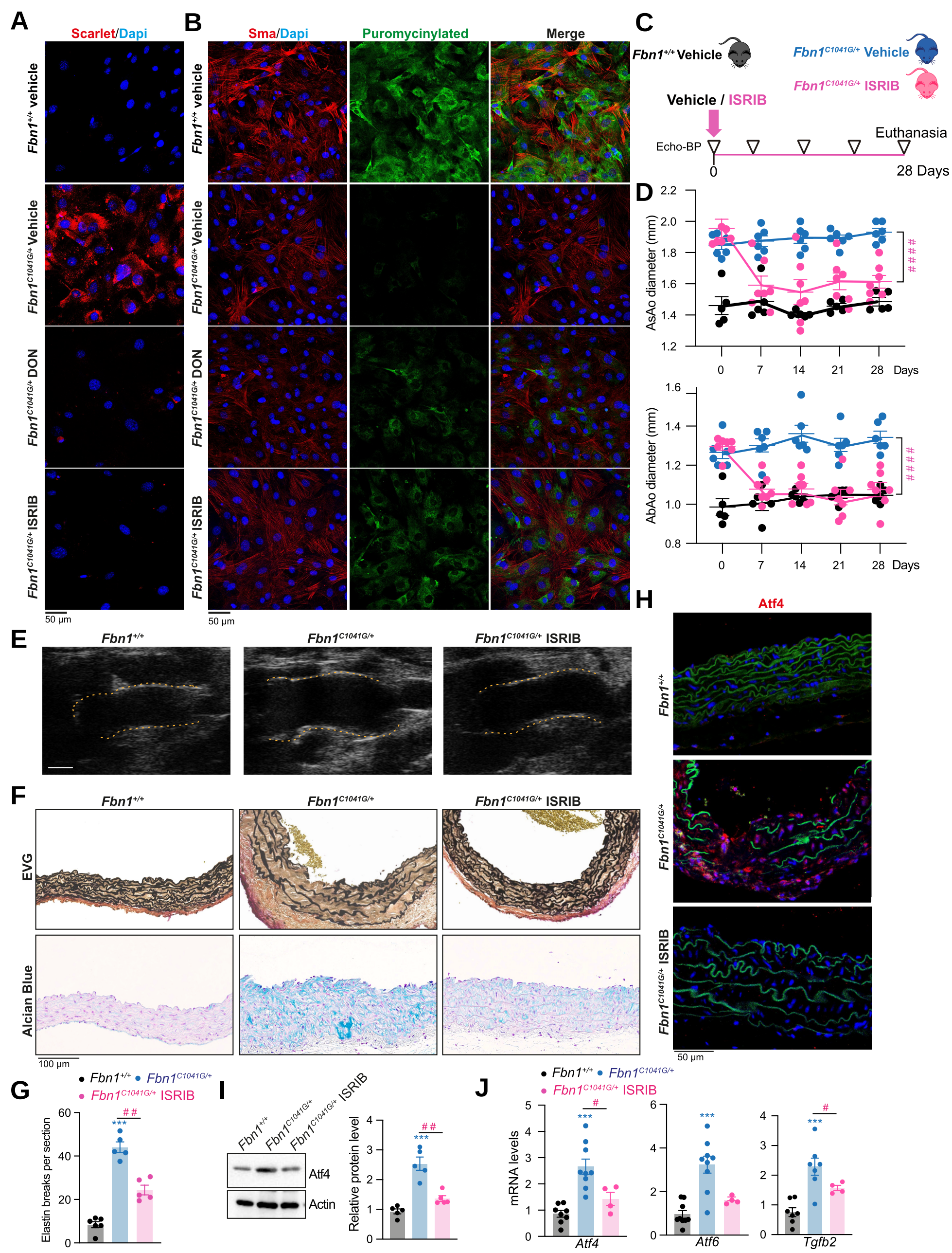

Figure 7 Integrated stress response contributes to vascular smooth muscle cells dysfunction and aortic pathology in Marfan syndrome mice. (*A*) Representative confocal imaging of Scarlet fluorescence in primary vascular smooth muscle cells from *Fbn1*$^{C1041G/+}$ and *Fbn1*$^{+/+}$ mice transduced with LV-ATF4Scarlet after 3 days treated with vehicle, 6-diazo-5-oxo-L-norleucine or integrated stress response inhibitor for 48 h ($n = 3$). (*B*) Representative confocal imaging of puromycinylated proteins and smooth muscle actin Sma, in primary vascular smooth muscle cells from *Fbn1*$^{C1041G/+}$ and *Fbn1*$^{+/+}$ mice incubated with puromycin for 5 min and treated with vehicle, 6-diazo-5-oxo-L-norleucine or integrated stress response inhibitor for 48 h ($n = 4$). (*C*) Experimental design, *A–E*, 20/22-week-old *Fbn1*$^{C1041G/+}$ and *Fbn1*$^{+/+}$ mice were infused with vehicle or integrated stress response inhibitor in minipumps for 28 days. (*D*) Evolution of maximal ascending (AsAo) and abdominal (AbAo) diameter. (*E*) Representative aortic ultrasound images after 28 days of control or integrated stress response inhibitor treatment. Discontinuous red lines mark the lumen boundary, scale bar 1 mm. (*F*) Representative histologic staining with Elastin van Gieson and Alcian blue in the AsAo and quantification of elastin breaks after 28 days of vehicle or integrated stress response inhibitor infusion (*G*). (*H*) Representative confocal imaging of Atf4, elastin (autofluorescence), and DAPI-stained nuclei in the ascending aorta from *Fbn1*$^{+/+}$ and *Fbn1*$^{C1039G/+}$ mice treated with/without integrated stress response inhibitor for 28 days ($n = 4$). (*I*) Representative immunoblot analysis and quantification of Atf4 in aortic extracts from *Fbn1*$^{C1041G/+}$ and *Fbn1*$^{+/+}$ mice with vehicle or integrated stress response inhibitor for 28 days. (*J*) Quantitative reverse transcription polymerase chain reaction analysis of *Atf4*, *Atf6*, and *Tgfb2* mRNA relative expression in aortic extracts from *Fbn1*$^{C1041G/+}$ and *Fbn1*$^{+/+}$ mice infused with vehicle or integrated stress response inhibitor for 28 days. Data are mean ± standard error of the mean. Two-way repeated measurements analysis of variance (*B*) or one-way analysis of variance (*G*, *J*, *I*) or $^{**}P < .01$, $^{***}P < .001$, for *Fbn1*$^{C1041G/+}$ vehicle vs *Fbn1*$^{+/+}$ vehicle; $\#P < .05$, $\#\#P < .01$, $\#\#\#\#P < .0001$ for *Fbn1*$^{C1041G/+}$ ISRIB vs *Fbn1*$^{C1041G/+}$ vehicle

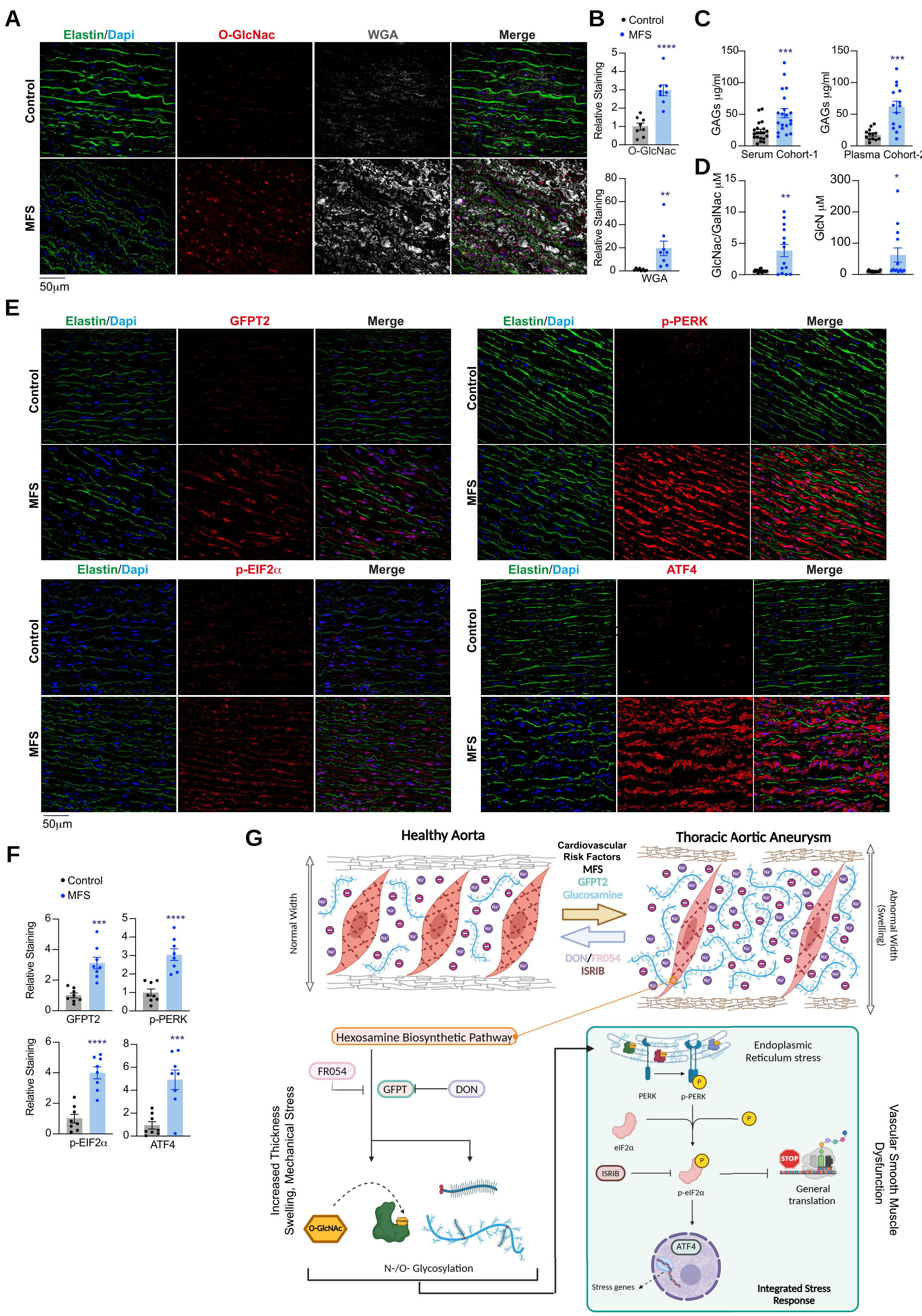

Figure 8 The HBP–ISR axis is up-regulated in Marfan syndrome patients. (*A*) Representative confocal immunostainings and quantification (*B*) of *O*-GlcNac (red) and wheat germ agglutinin (grey) elastin (green, autofluorescence), and DAPI-stained nuclei (blue) in medial layer of aortic sections from control donors or patients with Marfan syndrome ($n = 8$; $n = 4$ females, $n = 4$ males; per group). (*C*) Glycosaminoglycans serum and plasmatic levels, in two different cohorts of patients. (*D*) *N*-acetylglucosamine/*N*-acetylglucosamine and glucosamine levels in plasma from Cohort-2 of control or Marfan syndrome patients. (*E*) Representative confocal immunostainings and (*F*) quantification of GFPT2, p-PERK, p-EIF2α, ATF4, elastin (autofluorescence), and DAPI-stained nuclei in medial layer of aortic sections from control donors or patients with Marfan syndrome ($n = 8$; $n = 4$ females, $n = 4$ males; per group). (*G*) Proposed model depicting the differences between control and aortic pathology in Marfan syndrome and subsequent crosstalk of the HBP–ISR axis. Data are mean ± standard error of the mean, Student's *t*-test. *$P < .05$, **$P < .01$, ***$P < .01$ ****$P < .0001$ vs control

Inhibition of HBP by DON or FR054 reduced TGF-β-dependent gene expression in MFS aortas, suggesting HBP may reinforce TGF-β signalling in a feedforward loop. While no isoform-specific inhibitors for GFPT1 or GFPT2 are available, our data support the development of selective GFPT2-targeted therapies. Given that GFPT1 maintains basal HBP flux essential for homeostasis, selective inhibition of GFPT2 may provide a more specific strategy to block disease-associated glycosylation. However, the potential consequences of pharmacological inhibition or genetic deletion of GFPT2 remain unknown, and its exact role in cellular homeostasis is not fully understood.

UDP-GlcNAc fuels both *O*-GlcNAcylation and *N*-linked glycosylation. *O*-GlcNAcylation, catalysed by OGT, modifies cytoplasmic and nuclear proteins, often blocking phosphorylation. *O*/*N*-linked glycosylation occurs in the endoplasmic reticulum and Golgi, with further processing by MGAT enzymes and subsequent matrix secretion. Moreover, UDP-GlcNAc serves as a donor substrate for the biosynthesis of GAGs, including hyaluronic acid, heparan keratan, and chondroitin sulphate.[55–57] Increased expression of HAS1/3, GNE, and PGs in MFS suggests that HBP up-regulation drives ground substance accumulation in medial degeneration. Glycosaminoglycans and PGs are highly negatively charged molecules that play important roles in maintaining the structural integrity of the ECM. Their negative charge allows them to maintain electroneutrality by attracting cations such as Na^+, which in turn causes an influx of water molecules, leading to swelling of the aortic media. The accumulation of PGs and GAGs has profoundly deleterious consequences in the aortic media, as it breaks the delicate micromechanical equilibrium that allows for proper function of the elastic elements and optimal mechanotransduction by the VSMCs.[58–60] The interstitial content of PGs/GAGs in aortic media is essential to maintain a specific level of wall hydration, enabling it to withstand cyclic compression while concurrently sustaining tension in the elastic elements and their connections with VSMCs.[58] This emphasizes the importance of comprehending the structural alterations underlying aortic medial degeneration within the context of TAAD pathogenesis.[61] On the other hand, GAG and PG medial pooling disrupts VSMC anchorage, favouring phenotypic switch and Anoïkis.[62,63] Inhibiting HBP by DON has been shown to impact the ECM by reducing levels of thrombospondin, hyaluronic acid and collagen.[64,65] We observed reduced levels of GAGs and PGs by modulating vascular metabolism via DON or FR054 treatments. This reduction may alleviate stiffness, swelling, elastin breaks, and mechanical stress in the aorta, which might contribute to TAAD development. Further research is needed to fully elucidate the mechanisms by which GAGs and PGs contribute to aortic degeneration and how they interact with other components of the ECM to affect aortic biomechanics and integrity.[21,61]

Dynamic post-transcriptional *O*-GlcNAc modification of several cellular proteins plays a pivotal role in biological processes, including cell proliferation, autophagy, apoptosis, stress responses, epigenetics, metabolism, transcription, and protein trafficking.[33] Notably, important transcription factors implicated in TAAD pathogenesis, such as MYC, P53, and HIF1A,[25] are protected from degradation by *O*-GlcNac modification. Both types of glycosylation, along with their respective enzymes involved are increased in mouse and human TAAD aortas. However, further investigation is warranted to elucidate the specific roles of *O*-GlcNAc and *N*-linked glycosylation in different aspects of TAAD development. Our findings suggest that *N*-acetylhexosamines and GAGs levels are elevated in the blood of both mice and patients with MFS, suggesting their potential as molecular markers for TAAD disease. These elevated levels imply dysregulation in glycosylation pathways, likely contributing to the pathogenesis of TAAD. Further investigation is essential for identifying glycosylated proteins in blood and aortic tissue, as this may elucidate the two branches of the glycomics landscape within TAAD and their correlation with the stage of aortic degeneration. Such exploration holds promise for uncovering novel molecular pathways, biomarkers, and potential therapeutic targets.

We have observed that GlcN treatment increased HBP-derived glycosylation markers in wild-type mice to levels comparable with those found in MFS aortas. Furthermore, GlcN exacerbates aortic medial degeneration in MFS mice. Previous studies have shown that GlcN induces endoplasmic reticulum stress and consequently activates the ISR in the context of diabetic atherogenesis.[66] Additionally, GlcN is currently used as a dietary supplement to alleviate inflammation in osteoarthritis and joint pain in elderly patients, although its benefits remain unclear.[67] Given that many MFS patients suffer from joint pain, GlcN supplements might be recommended. However, despite using higher doses than typical supplements, our data raise concern about its potential vascular risk. Further studies are needed to assess the safety of GlcN in patients predisposed to vascular diseases.

Vascular ageing is noticeable by distinct histological changes, including arterial medial degeneration evidenced by medial calcification and disarray in elastin fibres.[68,69] Indeed, it has been described that HBP and *O*-GlcNac are increased in aortas, the heart, skeletal muscle, and the brain from aged rats.[70] Cardiac ageing is also associated with GAG accumulation secondary to increased HBP activity.[71] Previous studies relate senescence in MFS mice aortas.[25,72] Therefore, the augmentation of HBP throughout the ageing process might significantly contribute to vascular senescence and associated pathological features in TAAD.

Integrated stress response is activated by diverse cellular stresses, including endoplasmic reticulum stress, haem deficiency, viral infection, and amino acid deprivation, through four converging kinases.[73] Hexosamine biosynthetic pathway exhibits critical crosstalk with the endoplasmic reticulum stress and therefore, ISR pathways, playing a pivotal role in maintaining proteostasis.[26,39,71,74] Elevated HBP activity has been shown to promote ISR activation by increasing the phosphorylation of key mediators, such as PERK and eIF2α, canonical translation inhibition, and consequently leading to ATF4 translation.[29,75] In the context of TAAD, sustained ISR activation may lead to VSMC dysfunction and apoptosis. Although the precise mechanisms remain unclear, excessive HBP flux may alter endoplasmic reticulum homeostasis via hyperglycosylated protein aggregate accumulation. Further research is warranted to explore whether targeting ISR signalling may represent an effective therapeutic approach not only for TAAD but also for other vascular disorders such as cerebral or abdominal aortic aneurysms.[76,77] Understanding the broader role of the HBP–ISR axis in vascular disease may reveal novel therapeutic strategies.

Acknowledgements

The authors thank the staff members of the Cardiac Surgery Service at Fundación Jiménez Díaz University Hospital for their help in patients' recruitment and sample collection. The authors thank the plasma donors and the Hospital Universitario Puerta de Hierro Majadahonda (HUPHM)/Instituto de Investigación Sanitaria Puerta de Hierro-Segovia de Arana (IDIPHISA) Biobank (Carlos III Health Institute Biobanks and Biomodels Platform) for the human specimens used in this study. The authors acknowledge the patients and the Hospital Universitari Vall d'Hebron Biobank (PT20/00107) integrated in the Platform ISCIII Biobanks and Biomodels for their collaboration. They extend their sincere acknowledgements to the patients from SIMA (Spanish Marfan

Association). pLVX-ATF4 mScarlet NLS was a gift from David Andrews (Addgene plasmid # 115969; http://n2t.net/addgene:115969; RRID: Addgene_115969). They thank the CNIC histology facility and animal imaging facility. They thank the Cytometry Unit from CBMSO. They are also grateful to María del Mar González García-Parreño and Sandra Sanz de Andrés for technical support. The authors thank the Conchita Rábago Foundation for supporting A.R.-O, and Dr Borja Ibáñez for reagents and Dr Carmen Ayuso for manuscript review and scientific advice.

Supplementary data

Supplementary data are available at *European Heart Journal* online.

Declarations

Disclosure of Interest

All authors declare no disclosure of interest for this contribution.

Data Availability

The data, analytic methods, and study materials that support the findings of this study are available from the corresponding author on reasonable request.

Funding

A.R.-O. is supported by the Conchita-Rábago Foundation 2024 grant. J.O. is supported by a Ramón y Cajal contract (RYC2021-033343-I) and grant from Spanish Ministerio de Ciencia e Innovación grant (PID2022-137730OA-I00) funded by MCIN/AEI/10.13039/501100011033/FEDER, EU; granted by Fundación MERCK-FEDER 'Investigación clínica en enfermedades raras 2022', Marfan Spanish Association (SIMA, www.Marfan.es) and by 'V-Ayudas Muévete por los que no pueden 2021'. Research in M.M.'s lab was supported by European Research Council grant ERC-2021-CoG 101044248-LetTBe and the Y2020/BIO-6350 NutriSION-CM synergy grant from Comunidad de Madrid, Ministerio de Ciencia e Innovacion, Spain (grants PID2022-141169OB-I00 and PID2022-138295OB-I00). European Research Council. M.M.-L., G.A.-L., and G.A.-E. are funded by Instituto de Salud Carlos III through the projects PI20/01103, PI23/00100, and CP22/00100 (co-funded by European Regional Development Fund/European Social Fund 'A way to make Europe'/ 'Investing in your future'). J.L.M.-V. is supported by grant from Spanish Ministerio de Ciencia e Innovación (PID2022-136979OB-I00). L.M.B.-C. is supported by Fondo de Investigaciones Sanitarias, Instituto de Salud Carlos III (ISCIII/FEDER PI22/00233). G.T.-T. and A.G. are supported by Spanish Society of Cardiology (SEC/FEC-INV-CLI 20/015). O.L. is supported by grant from Spanish Health Ministry or Spanish Ministerio de Sanidad (PI20/00923 Instituto Carlos III). J.F.N. is supported by grant from Spanish Health Ministry or Spanish Ministerio de Sanidad (PI21/00084 FIS) and a grant from Health Research Institute Valdecilla (INNVAL21/24). N.M-B. is supported by Spanish Health Ministry or Spanish Ministeiro de Sanidad (PI21/01126). M.J.F.-G. is supported by Spanish Health Ministry or Spanish Ministerio de Sanidad contract (FIS22/00140). J.M.R. has received funding from La Caixa Foundation (HR18-00068); Spanish Ministerio de Ciencia e Innovación grant PID2021-122388OB-100 funded by MCIN/AEI/10.13039/501100011033; and Instituto de Salud Carlos III (CIBER-CV CB16/11/00264); Fundació La Marató TV3 grant 202334-31, and Spanish Ministerio de Ciencia e Innovación contract FPI (BES-2016-077649) to M.J.R.-R. The CBMSO is supported by Consejo Superior de Investigaciones Científicas and Universidad Autónoma de Madrid. CBMSO is a Severo Ochoa Centers of Excellence (grant CEX2021-001154-S) funded by MICIN/AEI/10.13039/501100011033.

Ethical Approval

Animal procedures and experiments complied with all relevant ethical regulations, were accredited by the CNIC and IIS-FJD Ethics Committee and the Madrid regional authorities (references PROEX 80/16, PROEX 74.7/23, PROEX 094.8/21), and conformed to EU Directive 2010/63/EU and Recommendation 2007/526/EC regarding the protection of animals used for experimental and other scientific purposes, enacted in Spanish law under Real Decreto 1201/2005. Mouse health was daily assessed for signs of discomfort; weight loss; or changes in behaviour, mobility and feeding, or drinking habits. The study complied with all relevant ethical regulations and was approved by the Clinical Research Ethics Committee of Cantabria (ref. 27/2013), the Ethics Committee of Instituto de Salud Carlos III (CEI PI91_2018-v2-Enmienda_2019 and CEI PI 65_2023) and Hospital Fundación Jiménez Díaz (HBP2023, PIC143-2016, PIC029-21, and PIC094-24_FJD) conformed to the principles set out in the WMA Declaration of Helsinki and the Department of Health and Human Services Belmont Report. Informed consent was obtained from all human participants or their families. Patient clinical data were retrieved while maintaining anonymity. For histological ascending aorta, samples used as controls were obtained anonymously from multi-organ transplant donors. During preparation of the heart for transplantation, excess AsAo tissue was trimmed and harvested for the study. Aortic samples and data from MFS patients included in this study were obtained during elective or emergency surgery for aortic root replacement and provided by the Hospital Universitari Vall d'Hebron Biobank (National Registry of Biobanks B.000018, PT20/00107). Tissues were immediately fixed, kept at room temperature for 48 h, and embedded in paraffin. Detailed patient characteristics, including mutation, medication, age, sex, and sample type, are presented in the Supplementary data. These samples were obtained and processed in accordance with standard operating procedures.

Pre-registered Clinical Trial Number

Not applicable.

References

1. Goldfinger JZ, Halperin JL, Marin ML, Stewart AS, Eagle KA, Fuster V. Thoracic aortic aneurysm and dissection. *J Am Coll Cardiol* 2014;**64**:1725–39. https://doi.org/10.1016/j.jacc.2014.08.025
2. Lindsay ME, Dietz HC. Lessons on the pathogenesis of aneurysm from heritable conditions. *Nature* 2011;**473**:308–16. https://doi.org/10.1038/nature10145
3. Pinard A, Jones GT, Milewicz DM. Genetics of thoracic and abdominal aortic diseases. *Circ Res* 2019;**124**:588–606. https://doi.org/10.1161/CIRCRESAHA.118.312436
4. Danyi P, Elefteriades JA, Jovin IS. Medical therapy of thoracic aortic aneurysms. *Trends Cardiovasc Med* 2012;**22**:180–4. https://doi.org/10.1016/j.tcm.2012.07.017
5. Dietz HC, Cutting GR, Pyeritz RE, Maslen CL, Sakai LY, Corson GM, *et al.* Marfan syndrome caused by a recurrent de novo missense mutation in the fibrillin gene. *Nature* 1991;**352**:337–9. https://doi.org/10.1038/352337a0
6. Milewicz DM, Braverman AC, De Backer J, Morris SA, Boileau C, Maumenee IH, *et al.* Marfan syndrome. *Nat Rev Dis Primer* 2021;**7**:64. https://doi.org/10.1038/s41572-021-00298-7
7. Keane MG, Pyeritz RE. Medical management of Marfan syndrome. *Circulation* 2008;**117**:2802–13. https://doi.org/10.1161/CIRCULATIONAHA.107.693523
8. Jana S, Hu M, Shen M, Kassiri Z. Extracellular matrix, regional heterogeneity of the aorta, and aortic aneurysm. *Exp Mol Med* 2019;**51**:1–15. https://doi.org/10.1038/s12276-019-0286-3

9. Michel J-B, Jondeau G, Milewicz DM. From genetics to response to injury: vascular smooth muscle cells in aneurysms and dissections of the ascending aorta. *Cardiovasc Res* 2018;**114**:578–89. https://doi.org/10.1093/cvr/cvy006
10. Lu H, Du W, Ren L, Hamblin MH, Becker RC, Chen YE, *et al.* Vascular smooth muscle cells in aortic aneurysm: from genetics to mechanisms. *J Am Heart Assoc* 2021;**10**: e023601. https://doi.org/10.1161/JAHA.121.023601
11. Stone JR, Bruneval P, Angelini A, Bartoloni G, Basso C, Batoroeva L, *et al.* Consensus statement on surgical pathology of the aorta from the Society for Cardiovascular Pathology and the Association for European Cardiovascular Pathology: I. Inflammatory diseases. *Cardiovasc Pathol* 2015;**24**:267–78. https://doi.org/10.1016/j.carpath.2015.05.001
12. Bahnson HT, Nelson AR. Cystic medial necrosis as a cause of localized aortic aneurysms amenable to surgical treatment. *Ann Surg* 1956;**144**:519–29. https://doi.org/10.1097/00000658-195610000-00002
13. Hukill PB. Healed dissecting aneurysm in cystic medial necrosis of the aorta. *Circulation* 1957;**15**:540–6. https://doi.org/10.1161/01.CIR.15.4.540
14. Yuan S-M, Jing H. Cystic medial necrosis: pathological findings and clinical implications. *Rev Bras Cir Cardiovasc* 2011;**26**:107–15. https://doi.org/10.1590/S0102-76382011000100019
15. Yin X, Wanga S, Fellows AL, Barallobre-Barreiro J, Lu R, Davaapil H, *et al.* Glycoproteomic analysis of the aortic extracellular matrix in Marfan patients. *Arterioscler Thromb Vasc Biol* 2019;**39**:1859–73. https://doi.org/10.1161/ATVBAHA.118.312175
16. Hirst AE, Gore I. Editorial: is cystic medionecrosis the cause of dissecting aortic aneurysm? *Circulation* 1976;**53**:915–6. https://doi.org/10.1161/01.CIR.53.6.915
17. Nataatmadja M, West M, West J, Summers K, Walker P, Nagata M, *et al.* Abnormal extracellular matrix protein transport associated with increased apoptosis of vascular smooth muscle cells in Marfan syndrome and bicuspid aortic valve thoracic aortic aneurysm. *Circulation* 2003;**108**:II329–34. https://doi.org/10.1161/01.cir.0000087660.82721.15
18. Carlson RG, Lillehei CW, Edwards JE. Cystic medial necrosis of the ascending aorta in relation to age and hypertension. *Am J Cardiol* 1970;**25**:411–5. https://doi.org/10.1016/0002-9149(70)90006-8
19. Wu D, Shen YH, Russell L, Coselli JS, LeMaire SA. Molecular mechanisms of thoracic aortic dissection. *J Surg Res* 2013;**184**:907–24. https://doi.org/10.1016/j.jss.2013.06.007
20. El-Hamamsy I, Yacoub MH. Cellular and molecular mechanisms of thoracic aortic aneurysms. *Nat Rev Cardiol* 2009;**6**:771–86. https://doi.org/10.1038/nrcardio.2009.191
21. Ghadie NM, St-Pierre J-P, Labrosse MR. The contribution of glycosaminoglycans/proteoglycans to aortic mechanics in health and disease: a critical review. *IEEE Trans Biomed Eng* 2021;**68**:3491–500. https://doi.org/10.1109/TBME.2021.3074053
22. Oller J, Gabandé-Rodríguez E, Roldan-Montero R, Ruiz-Rodríguez MJ, Redondo JM, Martín-Ventura JL, *et al.* Rewiring vascular metabolism prevents sudden death due to aortic ruptures—brief report. *Arterioscler Thromb Vasc Biol* 2022;**42**:462–9. https://doi.org/10.1161/ATVBAHA.121.317346
23. Marcos-Ríos D, Rochano-Ortiz A, San Sebastián-Jaraba I, Fernández-Gómez MJ, Méndez-Barbero N, Oller J. Mitochondrial dysfunction: a new hallmark in hereditable thoracic aortic aneurysm development. *Cells* 2025;**14**:618. https://doi.org/10.3390/cells14080618
24. Marcos-Ríos D, Rochano-Ortiz A, Méndez-Barbero N, Oller J. Defective mitochondrial respiration in hereditary thoracic aneurysms. *Cells* 2025;**14**:768. https://doi.org/10.3390/cells14110768
25. Oller J, Gabandé-Rodríguez E, Ruiz-Rodríguez MJ, Desdín-Micó G, Aranda JF, Rodrigues-Diez R, *et al.* Extracellular tuning of mitochondrial respiration leads to aortic aneurysm. *Circulation* 2021;**143**:2091–109. https://doi.org/10.1161/CIRCULATIONAHA.120.051171
26. Akella NM, Ciraku L, Reginato MJ. Fueling the fire: emerging role of the hexosamine biosynthetic pathway in cancer. *BMC Biol* 2019;**17**:52. https://doi.org/10.1186/s12915-019-0671-3
27. Paneque A, Fortus H, Zheng J, Werlen G, Jacinto E. The hexosamine biosynthesis pathway: regulation and function. *Genes (Basel)* 2023;**14**:933. https://doi.org/10.3390/genes14040933
28. Costa-Mattioli M, Walter P. The integrated stress response: from mechanism to disease. *Science* 2020;**368**:eaat5314. https://doi.org/10.1126/science.aat5314
29. Horn M, Denzel SI, Srinivasan B, Allmeroth K, Schiffer I, Karthikaisamy V, *et al.* Hexosamine pathway activation improves protein homeostasis through the integrated stress response. *iScience* 2020;**23**:100887. https://doi.org/10.1016/j.isci.2020.100887
30. Moore JA, Miller WP, Dennis MD. Glucosamine induces REDD1 to suppress insulin action in retinal Müller cells. *Cell Signal* 2016;**28**:384–90. https://doi.org/10.1016/j.cellsig.2016.01.017
31. Habashi JP, Judge DP, Holm TM, Cohn RD, Loeys BL, Cooper TK, *et al.* Losartan, an AT1 antagonist, prevents aortic aneurysm in a mouse model of Marfan syndrome. *Science* 2006;**312**:117–21. https://doi.org/10.1126/science.1124287
32. Campens L, Renard M, Trachet B, Segers P, Muino Mosquera L, De Sutter J, *et al.* Intrinsic cardiomyopathy in Marfan syndrome: results from in-vivo and ex-vivo studies of the Fbn1$^{C1039G/+}$ model and longitudinal findings in humans. *Pediatr Res* 2015;**78**: 256–63. https://doi.org/10.1038/pr.2015.110
33. Ong Q, Han W, Yang X. O-GlcNAc as an integrator of signaling pathways. *Front Endocrinol* 2018;**9**:599. https://doi.org/10.3389/fendo.2018.00599
34. Ryva B, Zhang K, Asthana A, Wong D, Vicioso Y, Parameswaran R. Wheat germ agglutinin as a potential therapeutic agent for leukemia. *Front Oncol* 2019;**9**:100. https://doi.org/10.3389/fonc.2019.00100
35. Franklin MK, Sawada H, Ito S, Howatt DA, Amioka N, Liang C-L, *et al.* β-Aminopropionitrile induces distinct pathologies in the ascending and descending thoracic aortic regions of mice. *Arterioscler Thromb Vasc Biol* 2024;**44**:1555–69. https://doi.org/10.1161/ATVBAHA.123.320402
36. Ishikita A, Matsushima S, Ikeda S, Okabe K, Nishimura R, Tadokoro T, *et al.* GFAT2 mediates cardiac hypertrophy through HBP-O-GlcNAcylation-Akt pathway. *iScience* 2021; **24**:103517. https://doi.org/10.1016/j.isci.2021.103517
37. Bolanle IO, Riches-Suman K, Williamson R, Palmer TM. Emerging roles of protein O-GlcNAcylation in cardiovascular diseases: insights and novel therapeutic targets. *Pharmacol Res* 2021;**165**:105467. https://doi.org/10.1016/j.phrs.2021.105467
38. Lemberg KM, Vornov JJ, Rais R, Slusher BS. We're not "DON" yet: optimal dosing and prodrug delivery of *6-Diazo-5-oxo-L-norleucine*. *Mol Cancer Ther* 2018;**17**:1824–32. https://doi.org/10.1158/1535-7163.MCT-17-1148
39. Ricciardiello F, Votta G, Palorini R, Raccagni I, Brunelli L, Paiotta A, *et al.* Inhibition of the hexosamine biosynthetic pathway by targeting PGM3 causes breast cancer growth arrest and apoptosis. *Cell Death Dis* 2018;**9**:377. https://doi.org/10.1038/s41419-018-0405-4
40. Sage AT, Walter LA, Shi Y, Khan MI, Kaneto H, Capretta A, *et al.* Hexosamine biosynthesis pathway flux promotes endoplasmic reticulum stress, lipid accumulation, and inflammatory gene expression in hepatic cells. *Am J Physiol Endocrinol Metab* 2010;**298**: E499–511. https://doi.org/10.1152/ajpendo.00507.2009
41. Nougarède A, Tesnière C, Ylanko J, Rimokh R, Gillet G, Andrews DW. Improved IRE1 and PERK pathway sensors for multiplex endoplasmic reticulum stress assay reveal stress response to nuclear dyes used for image segmentation. *ASSAY Drug Dev Technol* 2018;**16**:350–60. https://doi.org/10.1089/adt.2018.862
42. Anand AA, Walter P. Structural insights into ISRIB, a memory-enhancing inhibitor of the integrated stress response. *FEBS J* 2020;**287**:239–45. https://doi.org/10.1111/febs.15073
43. David A, Dolan BP, Hickman HD, Knowlton JJ, Clavarino G, Pierre P, *et al.* Nuclear translation visualized by ribosome-bound nascent chain puromycylation. *J Cell Biol* 2012;**197**:45–57. https://doi.org/10.1083/jcb.201112145
44. Schmidt EK, Clavarino G, Ceppi M, Pierre P. SUnSET, a nonradioactive method to monitor protein synthesis. *Nat Methods* 2009;**6**:275–7. https://doi.org/10.1038/nmeth.1314
45. Teixido-Tura G, Forteza A, Rodríguez-Palomares J, González Mirelis J, Gutiérrez L, Sánchez V, *et al.* Losartan versus atenolol for prevention of aortic dilation in patients with Marfan syndrome. *J Am Coll Cardiol* 2018;**72**:1613–8. https://doi.org/10.1016/j.jacc.2018.07.052
46. Forteza A, Evangelista A, Sánchez V, Teixidó-Turà G, Sanz P, Gutiérrez L, *et al.* Efficacy of losartan vs. Atenolol for the prevention of aortic dilation in Marfan syndrome: a randomized clinical trial. *Eur Heart J* 2016;**37**:978–85. https://doi.org/10.1093/eurheartj/ehv575
47. Rocha RV, Lindsay TF, Friedrich JO, Shan S, Sinha S, Yanagawa B, *et al.* Systematic review of contemporary outcomes of endovascular and open thoracoabdominal aortic aneurysm repair. *J Vasc Surg* 2020;**71**:1396–412.e12. https://doi.org/10.1016/j.jvs.2019.06.216
48. Tran DH, May HI, Li Q, Luo X, Huang J, Zhang G, *et al.* Chronic activation of hexosamine biosynthesis in the heart triggers pathological cardiac remodeling. *Nat Commun* 2020; **11**:1771. https://doi.org/10.1038/s41467-020-15640-y
49. Cork GK, Thompson J, Slawson C. Real talk: the inter-play between the mTOR, AMPK, and hexosamine biosynthetic pathways in cell signaling. *Front Endocrinol* 2018;**9**:522. https://doi.org/10.3389/fendo.2018.00522
50. He J, Li N, Fan Y, Zhao X, Liu C, Hu X. Metformin inhibits abdominal aortic aneurysm formation through the activation of the AMPK/mTOR signaling pathway. *J Vasc Res* 2021;**58**:148–58. https://doi.org/10.1159/000513465
51. Ding X, Liu H, Yuan Y, Zhong Q, Zhong X. Roles of GFPT2 expression levels on the prognosis and tumor microenvironment of colon cancer. *Front Oncol* 2022;**12**: 811559. https://doi.org/10.3389/fonc.2022.811559
52. Szymura SJ, Zaemes JP, Allison DF, Clift SH, D'Innocenzi JM, Gray LG, *et al.* NF-κB upregulates glutamine-fructose-6-phosphate transaminase 2 to promote migration in non-small cell lung cancer. *Cell Commun Signal* 2019;**17**:24. https://doi.org/10.1186/s12964-019-0335-5
53. Zhang W, Bouchard G, Yu A, Shafiq M, Jamali M, Shrager JB, *et al.* *GFPT2*-expressing cancer-associated fibroblasts mediate metabolic reprogramming in human lung adenocarcinoma. *Cancer Res* 2018;**78**:3445–57. https://doi.org/10.1158/0008-5472.CAN-17-2928
54. Tian Z, Zhang Y, Lyu X. Promoting roles of KLF5 in myocardial infarction in mice involving microRNA-27a suppression and the following GFPT2/TGF-β/Smad2/3 axis activation. *Cell Cycle* 2021;**20**:874–93. https://doi.org/10.1080/15384101.2021.1907512
55. Vigetti D, Viola M, Karousou E, De Luca G, Passi A. Metabolic control of hyaluronan synthases. *Matrix Biol* 2014;**35**:8–13. https://doi.org/10.1016/j.matbio.2013.10.002
56. Silbert JE, Sugumaran G. Biosynthesis of chondroitin/dermatan sulfate. *IUBMB Life* 2002; **54**:177–86. https://doi.org/10.1080/15216540214923

57. Ruiz-Rodríguez MJ, Oller J, Martínez-Martínez S, Alarcón-Ruiz I, Toral M, Sun Y, *et al.* Versican accumulation drives Nos2 induction and aortic disease in Marfan syndrome via Akt activation. *EMBO Mol Med* 2024;**16**:132–57. https://doi.org/10.1038/s44321-023-00009-7
58. Cikach FS, Koch CD, Mead TJ, Galatioto J, Willard BB, Emerton KB, *et al.* Massive aggrecan and versican accumulation in thoracic aortic aneurysm and dissection. *JCI Insight* 2018;**3**:e97167. https://doi.org/10.1172/jci.insight.97167
59. Shen YH, Lu HS, LeMaire SA, Daugherty A. Unfolding the story of proteoglycan accumulation in thoracic aortic aneurysm and dissection. *Arterioscler Thromb Vasc Biol* 2019; **39**:1899–901. https://doi.org/10.1161/ATVBAHA.119.313279
60. Roccabianca S, Ateshian GA, Humphrey JD. Biomechanical roles of medial pooling of glycosaminoglycans in thoracic aortic dissection. *Biomech Model Mechanobiol* 2014;**13**: 13–25. https://doi.org/10.1007/s10237-013-0482-3
61. Ghadie NM, Labrosse MR, St-Pierre J-P. Glycosaminoglycans modulate compressive stiffness and circumferential residual stress in the porcine thoracic aorta. *Acta Biomater* 2023;**170**:556–66. https://doi.org/10.1016/j.actbio.2023.08.061
62. Bunton TE, Biery NJ, Myers L, Gayraud B, Ramirez F, Dietz HC. Phenotypic alteration of vascular smooth muscle cells precedes elastolysis in a mouse model of Marfan syndrome. *Circ Res* 2001;**88**:37–43. https://doi.org/10.1161/01.RES.88.1.37
63. Michel J-B. Anoikis in the cardiovascular system: known and unknown extracellular mediators. *Arterioscler Thromb Vasc Biol* 2003;**23**:2146–54. https://doi.org/10.1161/01.ATV.0000099882.52647.E4
64. Raman P, Krukovets I, Marinic TE, Bornstein P, Stenina OI. Glycosylation mediates upregulation of a potent antiangiogenic and proatherogenic protein, thrombospondin-1, by glucose in vascular smooth muscle cells. *J Biol Chem* 2007;**282**:5704–14. https://doi.org/10.1074/jbc.M610965200
65. Chanmee T, Ontong P, Izumikawa T, Higashide M, Mochizuki N, Chokchaitaweesuk C, *et al.* Hyaluronan production regulates metabolic and cancer stem-like properties of breast cancer cells via hexosamine biosynthetic pathway-coupled HIF-1 signaling. *J Biol Chem* 2016;**291**:24105–20. https://doi.org/10.1074/jbc.M116.751263
66. Beriault DR, Werstuck GH. The role of glucosamine-induced ER stress in diabetic atherogenesis. *Exp Diabetes Res* 2012;**2012**:187018. https://doi.org/10.1155/2012/187018
67. Vo NX, Le NNH, Chu TDP, Pham HL, Dinh KXA, Che UTT, *et al.* Effectiveness and safety of glucosamine in osteoarthritis: a systematic review. *Pharmacy* 2023;**11**:117. https://doi.org/10.3390/pharmacy11040117
68. Sawabe M. Vascular aging: from molecular mechanism to clinical significance. *Geriatr Gerontol Int* 2010;**10**:S213–20. https://doi.org/10.1111/j.1447-0594.2010.00603.x
69. Clausen B. Influence of age on connective tissue. Hexosamine and hydroxyproline in human aorta, myocardium, and skin. *Lab Invest* 1962;**11**:229–34.
70. Fülöp N, Feng W, Xing D, He K, Nőt LG, Brocks CA, *et al.* Aging leads to increased levels of protein O-linked N-acetylglucosamine in heart, aorta, brain and skeletal muscle in Brown-Norway rats. *Biogerontology* 2008;**9**:139. https://doi.org/10.1007/s10522-007-9123-5
71. Grilo LF, Zimmerman KD, Puppala S, Chan J, Huber HF, Li G, *et al.* Cardiac molecular analysis reveals aging-associated metabolic alterations promoting glycosaminoglycans accumulation via hexosamine biosynthetic pathway. *Adv Sci (Weinh)* 2024;**11**: e2309211. https://doi.org/10.1002/advs.202309211
72. Hibender S, Franken R, van Roomen C, Ter Braake A, van der Made I, Schermer EE, *et al.* Resveratrol inhibits aortic root dilatation in the Fbn1$^{C1039G/+}$ Marfan mouse model. *Arterioscler Thromb Vasc Biol* 2016;**36**:1618–26. https://doi.org/10.1161/ATVBAHA.116.307841
73. Taniuchi S, Miyake M, Tsugawa K, Oyadomari M, Oyadomari S. Integrated stress response of vertebrates is regulated by four eIF2α kinases. *Sci Rep* 2016;**6**:32886. https://doi.org/10.1038/srep32886
74. Derisbourg MJ, Hartman MD, Denzel MS. Modulating the integrated stress response to slow aging and ameliorate age-related pathology. *Nat Aging* 2021;**1**:760–8. https://doi.org/10.1038/s43587-021-00112-9
75. Alhusban S, Nofal M, Kovacs-Kasa A, Kress TC, Koseoglu MM, Zaied AA, *et al.* Glucosamine-mediated hexosamine biosynthesis pathway activation uses ATF4 to promote "exercise-like" angiogenesis and perfusion recovery in PAD. *Circulation* 2024;**150**: 1702–19. https://doi.org/10.1161/CIRCULATIONAHA.124.069580
76. Chen B, Zhou H, Zhou X, Yang L, Xiong Y, Zhang L. Comprehensive analysis of endoplasmic reticulum stress in intracranial aneurysm. *Front Cell Neurosci* 2022;**16**:865005. https://doi.org/10.3389/fncel.2022.865005
77. Navas-Madroñal M, Rodriguez C, Kassan M, Fité J, Escudero JR, Cañes L, *et al.* Enhanced endoplasmic reticulum and mitochondrial stress in abdominal aortic aneurysm. *Clin Sci* 2019;**133**:1421–38. https://doi.org/10.1042/CS20190399